Evolution of the Plasma Universe: I. Double Radio Galaxies, Quasars, and Extragalactic Jets

ANTHONY L. PERATT, SENIOR MEMBER, IEEE

Abstract—**Cosmic plasma physics and our concept of the universe is in a state of rapid revision. This change started with *in-situ* measurements of plasmas in Earth's ionosphere, cometary atmospheres, and planetary magnetospheres; the translation of knowledge from laboratory experiments to astrophysical phenomena; discoveries of helical and filamentary plasma structures in the Galaxy and double radio sources; and the particle simulation of plasmas not accessible to *in-situ* measurement. Because of these, Birkeland (field-aligned) currents, double layers, and magnetic-field-aligned electric fields are now known to be far more important to the evolution of space plasma, including the acceleration of charged particles to high energies, than previously thought. This paper and its sequel investigate the observational evidence for a plasma universe threaded by Birkeland currents or filaments. This model of the universe was inspired by the advent of three-dimensional fully electromagnetic particle simulations and their application to the study of laboratory z pinches. This study resulted in totally unexpected phenomena in the data post-processed from the simulation particle, field, and history dumps. In particular, when the simulation parameters were scaled to galactic dimensions, the interaction between pinched filaments led to synchrotron radiation whose emission properties were found to share the following characteristics with double radio galaxies and quasars: power magnitude, isophotal morphology, spectra, brightness along source, polarization, and jets. The evolution of these pinched synchrotron emitting plasmas to elliptical, peculiar, and spiral galaxies by continuing the simulation run is addressed in a sequel paper.**

I. Introduction

COSMIC PLASMA physics is at present in a state of revision which is so rapid that it is appropriate to speak of a change in paradigm [1]–[3]. This change started a decade ago and is precipitated by the following.

a) *In situ* measurements of the properties of plasma in the magnetospheres, including the solar magnetosphere. Active space experiments are beginning to make significant contributions.

b) Laboratory investigations of plasmas with dimensions ranging from micrometers to centimeters have provided an increased understanding of how to transfer knowledge from one plasma region to another and from one size to another.

c) Recent discoveries including the observation of helical and filamentary structures in the galactic center and extragalactic radio sources.

d) Multidimensional particle-in-cell simulations. The solution to problems with complex geometry, intense self-fields, nonlinearity, nonhomogeneity, and explicit time dependence in both the laboratory and magnetosphere has instilled confidence that the electromagnetic particle-in-cell approach can be used to study plasmas not accessible to *in situ* measurement.

Because of these recent developments, our concept of cosmic plasma has changed considerably. Essential differences between the old and new paradigm include the following.

1) Electric double layers, which did not attract much attention a decade ago, are now known to accelerate charged particles to kilovolt energies in the terrestrial magnetosphere [4]–[7]. They may also exist elsewhere and accelerate particles to even higher energies.

2) The necessity of a global electric current description to describe the transfer of energy in magnetized cosmic plasmas. This leads to the necessity of drawing the circuits in which the current flows [8], [9]. (This approach also emphasizes the discrete particle description in simulating cosmic phenomena, where particle currents may be explicitly followed.)

3) In the magnetospheres, plasmas exist in both active and passive states; this is probably true for all cosmic plasmas.

4) Cosmic plasmas often are not homogeneous, but rather exhibit filamentary structures which are likely to be associated with currents parallel to the magnetic field.

5) In the magnetospheres there are thin stable current layers which separate regions of different magnetization, density, and temperature. Similar phenomena must also exist in more distant regions.

6) In the case where a current flows in a partially ionized plasma, a chemical separation may take place. Due to this and other effects, space plasmas have a general tendency to be separated into regions of different chemical composition.

The necessity of employing plasma physics to account for the observed electromagnetic radiation from cosmic sources has been pursued by a number of authors. In particular, Sturrock [10] and Sturrock and Barnes [11] proposed a magnetized plasma radiogalaxy model in which the tearing modes in current-conducting sheets play an important role in the radiation and morphologies observed. Alfvén postulates the existence of two neighboring double layers of radio lobe dimensions in a heliospheric pinched-current model involving the central elliptical galaxy [12]. The importance of pinched plasma

Manuscript received January 2, 1986; revised August 2, 1986.

The author is with Los Alamos National Laboratory, Los Alamos, NM 87545.

IEEE Log Number 8610981.

currents, beam instabilities, and filamentation to radio-galaxy processes has been pursued further by Peratt and Green [13], Browne [14], and also by Lerner [15], who points out the close similarities between measured radiation spectra from cosmic sources and that of the dense plasma focus and other pulsed power laboratory devices. Bostick's theory of radio sources is based on his dense plasma focus investigations [16].

This paper investigates the filamentary electric-current aspect of cosmic plasma. Section II describes the basic model: interactions among galactic-dimensioned field-aligned current filaments. Section III describes the analysis of the model with three-dimensional electromagnetic particle-in-cell simulations. The Biot–Savart force law for filaments is discussed in Section IV, while synchrotron radiation from pinched filaments is given in Section V. Sections VI and VII cover double radio sources, quasars, and magnetically confined sheet electron beams (jets). The author's conclusions are given in Section VIII. The evolution of cosmic plasma beyond the time frame investigated in this manuscript is presented in a sequel paper (denoted Paper II).

The only assumption made in the analysis in this paper—if it should be called an assumption—is that the basic properties of plasmas are the same everywhere, from submillimeter dimensions to the Hubble distance (10^{28} cm) [1]–[3], [8], [9].

II. Basic Model: Galactic-Dimensioned Birkeland Filaments

An electromotive force $V = \int \boldsymbol{v} \times \boldsymbol{B} \cdot d\boldsymbol{s}$ giving rise to electrical currents in conducting media is produced wherever a relative perpendicular motion of plasma and magnetic-field lines exist [8], [17]–[19]. An example of this is the (nightside) sunward-directed magnetospheric plasma that cuts the earth's dipole field lines in the equatorial plane, thereby producing a potential supply that drives currents within the auroral circuit. The tendency for charged particles to follow magnetic lines of force and therefore produce field-aligned currents has resulted in the widespread use of the term "Birkeland currents" in space plasma physics [20], [21]. Their discovery in the earth's magnetosphere in 1974 has resulted in a drastic change in our understanding of aurora dynamics, now attributed to the filamentation of Birkeland charged-particle sheets following the earth's dipole magnetic-field lines into vortex current bundles. In anticipation of the importance of Birkeland currents in astrophysical settings, Fälthammar states [22]:

> "A reason why Birkeland currents are particularly interesting is that, in the plasma forced to carry them, they cause a number of plasma physical processes to occur (waves, instabilities, fine structure formation). These in turn lead to consequences such as acceleration of charged particles, both positive and negative, and element separation (such as preferential ejection of oxygen ions). Both of these classes of phenomena should have a general astrophysical interest far beyond that of understanding the space environment of our own Earth."

A. Birkeland Currents in Laboratory Plasma

In the laboratory, filamentary structure is a common morphology exhibited by energetic plasmas. X-ray pinhole photographs, optical streak and framing camera photographs, and laser holograms often show a filamentary magnetic "rope-like" structure from plasmas produced in multiterawatt pulse power generators or in dense plasma focus machines. High-resolution etchings of electron beams onto witness plates show nearly identical vortex profiles ranging from a dimension of a few micrometers in the dense plasma focus, to a few centimeters in cathode electron beams [23]–[26]. This size variation of four orders of magnitude is extended to nearly nine orders of magnitude when auroral vortex recordings are directly compared to the laboratory data [27]. With regard to actual current magnitudes, fine-detail resolution of current filaments shows indistinguishable vortex patterns over nearly 12 orders of magnitude while coarser resolution shows that the phenomena probably transcend at least 14 orders of magnitude, from microampere to multimegaampere electron beams.

B. Birkeland Currents in Cosmic Plasma

As far as we know, most cosmic low-density plasmas also depict a filamentary structure. For example, filamentary structures are found in the following cosmic plasmas, all of which are observed to be associated with or are likely to be associated with electric currents.

1) In the aurora, filaments parallel to the magnetic field are very often observed. These can sometimes have dimensions down to about 100 m.

2) Inverted V events and the *in-situ* measurements of strong electric fields in the magnetosphere (10^5–10^6 A, 10^8 m) demonstrate the existence of filamentary structures.

3) In the ionosphere of Venus, "flux ropes," whose filamentary diameters are typically 20 km, are observed.

4) In the sun, prominences (10^{11} A), spicules, coronal streamers, polar plumes, etc., show filamentary structure whose dimensions are of the order 10^7–10^8 m.

5) Cometary tails often have a pronounced filamentary structure [28].

6) In the interstellar medium and in interstellar clouds there is an abundance of filamentary structures, e.g., the Veil nebula, the Lagoon nebula, the Orion nebula (Fig. 1), the Crab nebula, etc.

7) The center of the Galaxy, where twisting plasma filaments, apparently held together by a magnetic field possessing both azimuthal and poloidal components, extend for nearly 500 light years (5×10^{18} m) [29].

8) Within the radio bright lobes of double radio galaxies, where filamental lengths may exceed 20 kpc (6×10^{20} m) [30].

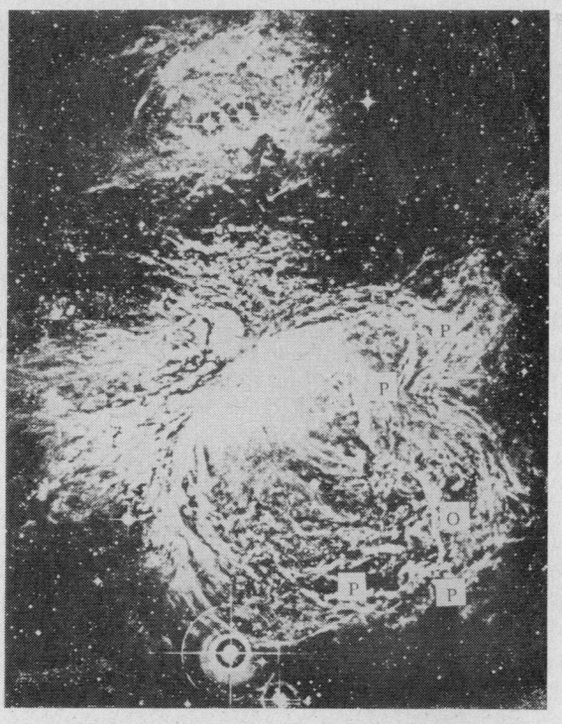

Fig. 1. Detail of the Orion nebula (*Sky and Telescope*, Nov. 1979). This paper investigates what an observer at *O* would see when looking into filamental interactions at points *P* in a plasma universe of similar structure.

C. The Formation of Double Layers Within Birkeland Currents

Recent literature in the area of magnetospheric physics reflects considerable interest in magnetic-field-aligned electric fields. Such electric fields can have important consequences in cosmic plasma [31], [32], including the "unfreezing" of magnetic fields, the acceleration of electrons to very high energies, and the filamentation of the plasma itself.

In magnetized nonhomogeneous astrophysical plasma, a number of mechanisms are present that can generate field-aligned electric fields. These include anomolous resistivity caused by wave–particle interactions, collisionless thermoelectric effect due to energy-dependent wave–particle interactions, magnetic mirror effects involving trapped particles and magnetic-field gradients, and electric double layers due to localized charge separation. While all of the above mechanisms have been studied in the laboratory and simulated by computer, it is the last mechanism that has been found to be remarkably prolific in producing appreciable potential drops in neutral plasma. Moreover, Birkeland currents and double layers appear to be associated phenomena, and both laboratory experiments [33] and computer simulations [34] have shown the formation of a series of double layers along current-carrying plasma columns or filaments. Fig. 2 illustrates the geometry at hand. When double layers (or a series of double layers) form in adjacent Birkeland current filaments, field-aligned electric fields are generated, which then serve to accelerate electrons within these regions.

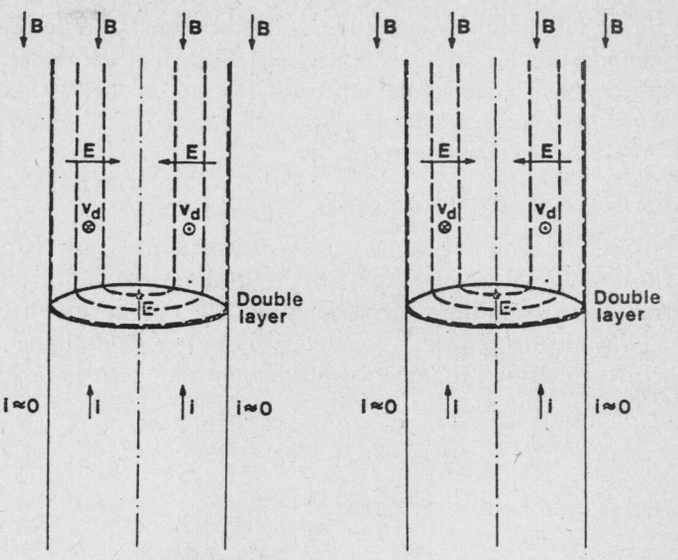

Fig. 2. Double layers in adjacent Birkeland current filaments.

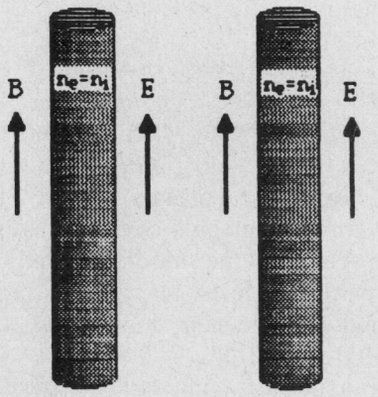

Fig. 3. Basic geometry under consideration; two parallel Birkeland currents.

D. Interacting Birkeland Currents Model

It is the purpose of this paper to extend the study of cosmic plasma to the case of galactic-dimensioned (50 kpc in width) Birkeland filaments by means of three-dimensional, fully electromagnetic, and relativistic particle-in-cell simulations. Fig. 1 is a contrast-enhanced photograph of the Orion nebula but serves the purpose of representing the morphology to be expected by an observer situated within a much larger filamentary metagalactic structure.

The simulation model consists of modeling a magnetic-field-aligned neutral plasma filament (column) in the presence of a field-aligned electric field. (Strictly speaking, because of the parallel electric field, the portion of the filament simulated is a double layer [35].) To study the evolution of interacting filaments, a second filament (nearly identical to the first) is placed adjacent as depicted in Fig. 3. (As many as six filaments have been investigated by simulation while up to 12 filaments have been studied experimentally. However, because of the r^{-1} force between filaments, it would appear that a majority of cosmic plasma phenomena are the result of two, or at most

three, interactions among the closest filaments.) The remainder of this paper is concerned with what the signatures of existence would be to an observer situated within a nonhomogeneous plasma universe consisting of galactic-sized Birkeland currents.

III. Simulation Parameters

Specification of plasma density, temperature, magnetic field strength, acceleration field, and filamental width set the initial conditions for simulation. The parameters that delineate the physical characteristics of a field-aligned current-carrying filament of plasma are the electron drift velocity

$$\beta_z = v_z/c \tag{1}$$

the plasma thermal velocity

$$\beta_{th} = v_{th}/c = \frac{(\lambda_D/\Delta)(\omega_p dt)}{cdt/\Delta} \tag{2}$$

and the thermal/magnetic pressure ratio

$$\beta_p = \frac{n_e kT_e + n_i kT_i}{B^2/2\mu_0} = \frac{[(\omega_p dt)(\lambda_D/\Delta)]^2\, 4(1 + T_i/T_e)}{(cdt/\Delta)^2\, [(\omega_{c0}/\omega_p)^2]} \tag{3}$$

where $n_e = n_i$ is the neutral plasma density, T is the plasma temperature, k is Boltzmann's constant, μ_0 is the permeability of free space,and the subscripts e and i denote electron and ion particle species, respectively. The parameter dt is the simulation time step, Δ is the cell size, and c is the speed of light.

We choose a plasma temperature typical for cosmic Birkeland filaments, a few kiloelectronvolts [31], by setting the initial dimensionless simulation parameters to $\omega_p dt = 0.25$ (electron plasma frequency), $\lambda_D/\Delta = 0.25$ (the Debye length in cells), and $cdt/\Delta = 1.0$ (the speed of light). A field-aligned Birkeland filament is established by means of the parameter $\omega_{c0}/\omega_p = 1.5$ where $\omega_c 0 = eB_{z0}/m_e$ and $B_{z0} = B(t = 0)$ is the axial magnetic field. For this choice of parameters, $\beta_{\text{th}} = 0.0625$ and, for $T_e = T_i$, $\beta_p = 0.0069$. Current flow within the filament is initiated by setting $E_{z0}/B_{z0} = 0.01c$, so that $0 \le \beta_z \le 1$.

The simulations are carried out with the three-dimensional electromagnetic particle codes SPLASH and TRISTAN [36]. The former code consists of 32 768 cells and 250 000 particles while the latter code has 4 194 304 cells, 2 million photons, and 5 million particles. For SPLASH, the radius of each filament is 3Δ and the center-to-center separation is 11Δ, while for TRISTAN the radius and separation are 12Δ and 44Δ, respectively.

SPLASH has been benchmarked against the $m = 1$ helical instability in magnetized z pinches [37], interacting plasmoids [38], microampere to submegaampere cylindrical charged particle beams [26], thin-sheet beam propagation experiments [39], auroral magnetic storms [39], and barium plasma experiments in the magnetosphere [40].

IV. Biot–Savart Forces Between Filaments

Because of the EMF-induced current I_z, a galactic filament can be expected to retain its columnar filamental form provided the Bennett-pinch condition is satisfied, i.e., that

$$I_z^2 > 8\pi NkT/\mu_0 \tag{4}$$

where N is the electron density per unit length [41].

In addition to confining plasma in filaments radially, the axial current flow produces another important effect; a long-range interactive force on other galactic filaments [2], [13], [38]. The Biot–Savart electromagnetic force between filaments is

$$\boldsymbol{F}_{21} = \int \boldsymbol{j}_2 \times \boldsymbol{B}_{21} d^3 r \tag{5}$$

for all space, where $\boldsymbol{j} \times \boldsymbol{B}$ is the Lorentz force. If the current path greatly exceeds the filament widths, the attractive force between two similarly oriented filaments is approximately given by

$$F_{21}(I_{z1}, I_{z2}) = -\boldsymbol{r}\frac{\mu_0 I_{z1} I_{z2}}{2\pi R_{12}} \tag{6}$$

where the subscripts 1 and 2 denote columns 1 and 2, respectively, and R_{12} is their separation. Because of the axial magnetic field B_z, the particles spiral as they drift or accelerate and thereby produce an azimuthal component in the generalized current $\boldsymbol{I} = zI_z + \theta I_\theta$. The magnetic moment associated with the azimuthal current is $\boldsymbol{m} = zB_z R^3 = z\pi R^2 I_\theta$. If the magnetic moments in adjacent filaments are aligned, a short-range repulsive force is generated between them:

$$F_{21}(I_{\theta 1}, I_{\theta 2}) = \boldsymbol{r}\frac{m_1 m_2}{R_{12}^4}. \tag{7}$$

Hence, the electromagnetic forces between filaments are ordered as R_{12}^{-1} (long-range attractive) and R_{12}^{-4} (short-range repulsive).

During long-range attraction, the motion of either filament in the interaction region may be approximately described by the equation $Mdr^2/dt^2 = \mu_0 I_z^2 L/4\pi(a - r)$, the solution of which is

$$v = dr/dt = I_z(\mu_0 L/2\pi M)^{1/2}\,(\ln a/a - r)^{1/2} + v(0) \tag{8}$$

where L is the length of the filamental region involved in Biot–Savart attraction, M is the total mass, $2a$ is the distance of separation between filaments, and $v(0)$ is the relative velocity at time zero. For the case $v(0) = 0$, and if the filaments are sufficiently separated so that the logarithmic correction is of order unity, the velocity is approximately given by

$$v \approx I_z(\mu_0 L/2\pi M)^{1/2}$$

$$\{v \approx I_z(2L/c^2 M)^{1/2} = B_\theta d/2\sqrt{2L/M}\}_{\text{CGS}}. \tag{9}$$

In dimensionless gaussian simulation units, (9) is

$$v = B_\theta d/2\sqrt{2L/M} \tag{10}$$

where $\mathbb{M} = N_c(n_e/\Delta^3)(m_i/m_e + 1)\pi\mathbb{r}_c^2\mathbb{L}$ and N_c are the total simulation mass and number of interacting simulation filaments, respectively. The parameter $\mathbb{d} = d/\Delta$ is the distance between filaments in cell widths, $\mathbb{r}_c = r_c/\Delta$ is the radius of a filament in cell widths, and

$$\mathbb{B} = B/(\mathrm{mc}\omega_p/e) = \omega_c/\omega_p \tag{11}$$

is the magnetic field in dt time steps (for $B = B_\theta$).

V. Synchrotron Radiation from Bennett-Pinched Filaments

A. The Application of the Synchrotron Mechanism to Cosmic Plasma

One of the most important processes that limit the energies attainable in particle accelerators is the radiative loss by electrons accelerated by the magnetic field of a betatron or synchrotron. This mechanism was first brought to the attention of astronomers by Alfvén and Herlofson [42]; a remarkable suggestion at a time when plasma, magnetic fields, and laboratory physics were thought to have little, if anything, to do with a cosmos filled with "island" universes (galaxies). While the Alfvén–Herlofson proposal was cast in terms familiar to astronomy, it is clear that the suggestion pertained to radiative emission of relativistic electrons in the trapping field of the interstellar magnetic field, or in an intergalactic magnetic field.

Synchrotron radiation is characterized by a generation of frequencies appreciably higher than the cyclotron frequency of the electrons, a continuous spectra (for a population of electrons) whose intensity decreases with frequency beyond a critical frequency (near-intensity maxima), increasing beam directivity with increasing γ ($\gamma = (1 - \beta_z^2)^{-1/2}$), and strongly polarized electromagnetic wave vectors. Many excellent reviews of synchrotron radiation in laboratory and astrophysical sources are to be found in the literature [43]–[50].

The recognition that this mechanism of radiation is important in astronomical sources has been one of the most fruitful developments in astrophysics. For example, it has made possible the inference that high-energy particles exist in many types of astronomical objects; it has given additional evidence for the existence of extensive magnetic fields; and it has indicated that enormous amounts of energy may indeed be generated, stored, and released in cosmic plasma.

B. Experimental Studies of Synchrotron-Emitting Bennett Pinches

Charged particle beams held together or pinched by their self-magnetic fields have been of general interest since their earliest investigation by Bennett [41]. The macroscopic picture of such a beam is that of a self-consistent magnetic confinement or compression against the expansion due to thermal pressure (4). On the microscopic scale, the individual particle orbits include radial oscillations due to the Lorentz force superimposed on the drift in the direction of mean flow. These are the betatron oscillations. Since they imply particle acceleration, there is electromagnetic radiation associated with them. Because the force is a $\boldsymbol{v} \times \boldsymbol{B}$ force, the radiation from the relativistic electrons is synchrotron radiation.

Manifestations of the pinch effect appear for a laboratory observer as a rapidly occurring phenomenon. A burst of radiation from high-current discharges (with current densities of the order 10^{11} A/cm^2), such as low-inductance vacuum sparks, plasma focus devices, and exploded wires is found over a broad spectral range: from the microwave region to the hard X-ray region [51]–[54]. Recorded data show that the radiation bursts are correlated with dips in the current waveform, i.e., interruptions in the current flow. Analysis of the directional patterns of the millimeter radiations shows that the microwave radiation is synchrotron radiation of electrons in the magnetic field of the proper current. The hard X-ray quanta are attributed to synchrotron radiation from the electrons at the transitions between Landau levels in this same current-induced magnetic field [55].

The total synchrotron power radiated incoherently from a Maxwellian distribution of electron velocities, over all frequencies, is given by [56]

$$p_{\mathrm{syn}} = \left\{\frac{4_e^4}{3m_e^2c^3} B^2 n_e \beta_z^2\right\}_{\mathrm{CGS}}, \quad \mathrm{ergs/cm^3}. \tag{12}$$

Similar expressions applicable for the determination of the average power radiated per unit length for relativistic Bennett pinches have been given by Meierovich [55] and Newberger [57], [58].

An enhancement of radiated power, given by (12), is achieved when the sum of the $\boldsymbol{v} \times \mathbf{B}$ radial forces seen by the relativistic electrons (5) is increased, as is the case when the azimuthal magnetic fields of neighboring pinches are present. While no theoretical treatment of synchrotron enhancement from beam interactions is known, this phenomenon has been examined in some detail, both experimentally and with simulations.

Fig. 4(a) illustrates the radiation yield versus the number of columnar Bennett-pinched plasma filaments. The experimental data (solid dots) pertain to 30-mm-long 15-μ-diameter metallic wires strung between the cathode and anode of a terawatt pulse-power generator [25]. In all cases, the delivered pulse is approximately 50 ns long, while the radiation burst duration is approximately 5 ns long. As illustrated, an X-ray energy enhancement of 6 is obtained when two filaments interact and enhancement factors -12–30 are recorded when up to 12 filaments symmetrically arrayed about a common center interact. Laser shadowgraphy diagnostics have shown the following sequence of events leading to broad-band electromagnetic radiation in pulsed power. Before the current reaches a value sufficient to fully establish the Bennett pinch (4) in the conducting filaments, plasma flows off the filaments towards the geometrical center along a path defined by the magnetic separatrix (see Section VII). The subsequent collision (interaction) of the inflowing plasma is photographically recorded in the emission of X rays by means

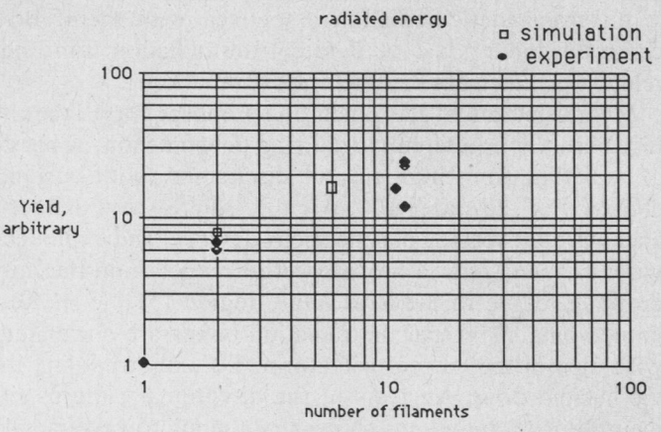

(a)

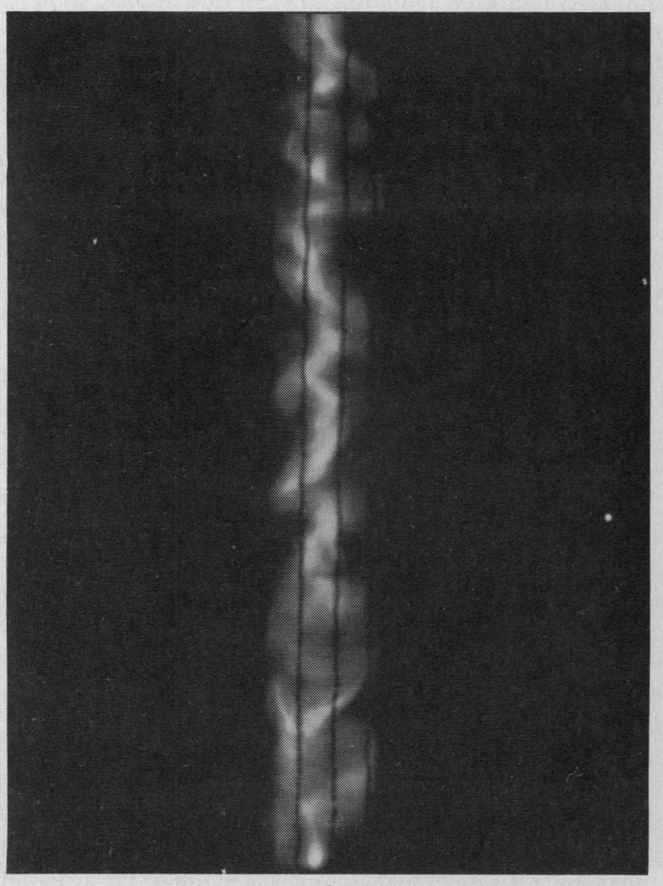

(b)

Fig. 4. (a) Radiated energy versus number of filaments. Solid dots—K-shell X-ray energy for 1 MV, 1.3 MA delivered to single wire and wire array loads. Hollow dots—splash simulation. (b) X-ray pinhole photograph (seen side-on) of plasma trapped in the magnetic sump between wires [25]. Wire filaments in absorption of X rays from the central emitting region are observable in the photograph. While the wire length exceeds the array diameter for the laboratory case, a double-layer-produced electric field within a galaxy may be of the order of or smaller than the distance between interacting Birkeland currents.

of pinhole cameras using X-ray film plates. The photographs show the topology of the emitting plasma configuration during the 5-ns burst, as-well-as the absorption profiles of the filamental pinches in between the camera and the emitting plasma, and the radiation "lit" surfaces of the filamental pinches behind the emission region. Fig.

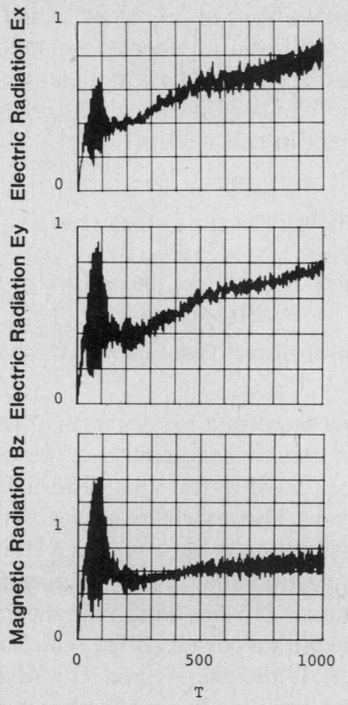

Fig. 5. Simulation synchrotron radiation characteristics for two interacting current-carrying filaments.

4(b) shows that the morphology of the radiating plasma, at radiation burst, is both helical and filamentary. This structure and the radiation enhancement is recorded only when the number of wires is greater than 1, i.e., the wires are interacting electromagnetically. The helicity is extremely well defined in some X-ray photographs and demonstrates the presence of an axial component to the magnetic field, even if none is externally imposed initially. (The second paper in [23] shows in a contact print on CR39 etchable plastic track detector a vortex pattern when no axial B_{0z} field was used in the plasma focus. This shows how the same morphology can be delineated using a totally different technique.) Late time-streak and framing camera diagnostics show the Biot–Savart attraction, rotation, and coalescence of the dense filaments themselves [25].

C. Simulation Studies of Synchrotron-Emitting Bennett Pinches

Fig. 5 is a plot of the simulation electric and magnetic energies lost as synchrotron radiation in arbitrary energy units (AEU) versus time in inverse units of plasma frequency ω_p^{-1} [37].[1] Whenever the attractive force between simulation columns causes their separation to be reduced to a distance such that the repulsive force (7) starts to become comparable to the attractive force (6), a burst in the radiation occurs (Fig. 5). For the parameters used in these simulations, this distance is of the order of several

[1]The author thanks a referee for pointing out that the arbitrary energy unit is not quite arbitrary, but corresponds to the total initial particle thermal energy.

pinch radii. As shown in Fig. 5, the radiation from the kiloelectronvolt particles is polarized in the transverse plane and the synchrotron enhancement (burst) is detected in the x and y electric radiation energies (W_{ERx}, W_{ERy}) and the z magnetic radiation energy (W_{BRz}). The burst lasts until the induced axial magnetostatic energy W_{Bz}, due to the azimuthal current θI_θ, is depleted (because the counterparallel azimuthal current force (7) brakes the azimuthal electron flow in both filaments). For some simulational parameters, W_{Bz} can build up and discharge again in the form of additional bursts of synchrotron radiation. The long-time slowly varying increase in radiation in W_{ERx} and W_{ERy} is due to the buildup of electrostatic energy from charge separation in the particle number and size constrained simulation model.

VI. Double Radio Sources

The existence of double radio galaxies presents a major challenge to cosmological theories. The discovery of discrete radio sources dates back to the pioneering survey of Reber (1944), who found two areas of enhanced intensity in Cygnus and Cassiopeia [59]–[62]. Cygnus A, the brightest radio source in the constellation Cygnus, has proved to be the "prototype" of double radio galaxies, and models of double radio galaxies are usually based on the characteristics of this source. Many excellent reviews on the properties of double radio sources observed from the 1960's on are available in the literature [63]–[66], as are a number of models of sources. However, regardless of whatever ingredients are postulated as necessary in models used to "explain" their existence, what is observed from any radio source is synchrotron radiation, which requires only the presence of relativistic electrons in a magnetic field.[2]

A. Requirements of the Model

Any plausible theory on double radio galaxies should be expected to explain the following:

a) the origin and source of energy of double radio galaxies;
b) the total magnitude of the radio flux observed;
c) the measured flux density as a function of frequency;
d) the observed isophotal morphologies;
e) the spatially varying power law within a source;
f) the polarization properties of the incoherent synchrotron radiation measured; and
g) the lifetime and evolution of a source.

[2]In addition to the model described in this paper, there are at least two other related plasma models of double radio galaxies. Alfvén proposes a circuit on the galactic scale where the current is driven by the dynamo action of a rotating galaxy. Inside the galaxy, the current flows in the plane of symmetry; outside, it follows back to the plane of symmetry. Alfvén suggests that double layers may occur in the axial parts of the circuit on either side of the central galaxy, leading to double radio lobe emission regions. Bostick proposes a model where electromagnetically attracting plasmas join to make a bar which is the armature of a homopolar generator. Two plasma foci at the center of the armature shoot jets of plasma perpendicular to the galactic plane, each of which terminates in a radio lobe. Additionally, in d) it is also necessary to explain the radiation "hot spots" in classical radio doubles; their diametric displacement off an imaginary axis running from giant radio lobe to giant radio lobe through an elliptically shaped center; the relationship between "bridges" and so-called jets connecting the elliptical center with the lobes; the one-sidedness of jets in quasars and powerful sources; multiknotted features in hot spots, bridges, and jets; the apparent superluminosity of some sources; and the problem of a nearly uniformly fading of some jets, thousands of light years in extent, in a few decades.

B. Scaling Simulations to Galactic Dimensions

The scaling of plasma physics on cosmical and laboratory scales generally involves estimates of the diffusion in plasma, inertia forces acting on the currents, the Coriolis force, the gravitational force, the centrifugal force, and the $\boldsymbol{j} \times \boldsymbol{B}$ electromagnetic force [67], [68]. The simulations reported in this paper are scaled to Cygnus A using the latter force law via (9).

Cygnus A consists primarily of two radio lobes of dimension $l \cong w \cong 10^{21}$ m (35 kpc) separated on either side of an elliptical galaxy by a distance $a \cong 1.22 \times 10^{21}$ m [43]–[46], [63]–[66], [69]–[72]. Typically, estimates of the relative velocities between cosmic plasmas range from hundreds of kilometers per second to 1000–8000 km/s (for interactions between components of peculiar galaxies [73]). Random velocities characteristic of the velocity dispersion of galaxies in highly condensed clusters are of the order 2000 km/s [74], [75]. Assuming a total plasma mass for the radio lobes of Cygnus A of the order of that observed in galaxies, $M \cong 10^{41}$ kg (while noting that all mass estimates are model dependent), and setting the velocity of attraction between filaments to 1000 km/s, yields $I_z \cong 2.15 \times 10^{19}$ A and $B_\theta = \mu_0 I_z / w \cong 2.5 \times 10^{-8}$ T (2.5×10^{-4} G). (The quantities I_z and B_θ are physically nonsensitive to the actual mass distribution, depending only on the square root of the mass per unit length; a slower velocity of 1000 km/s is chosen since this velocity increases with increasing current as the source develops in time.)

To convert simulation results to dimensional form, it is sufficient to fix the value of one physical quantity, e.g., B_θ. Since we are scaling to the strong radio source Cygnus A, the value of B_θ is applied at time step 90, the peak synchrotron burst energy. At this time, B_θ has grown comparable in strength to B_{z0} so that $\beta_p = 0.0034$. Velocity counts show $T_\perp \approx 2.8$ keV at time $T = 90$. Substituting β_p, $T_\perp$, and B into (3) yields a mean plasma density $n_e = 1.79 \times 10^3$ m^{-3} (1.7×10^{-3} cm^{-3}). Since $\omega_{c0}/\omega_p = 1.5$, the axial magnetic field strength is $B_{z0} = 2.0 \times 10^{-8}$ T (2.0×10^{-4} G). These parameter values characterize Cygnus A and are in close agreement with many previously published estimates using independent means (Table I). Additionally, from the simulation parameter $E_{z0}/B_{z0} = 0.01c$, the acceleration field within a filament is $E_{z0} = 63.4$ mV/m.

TABLE I
COMPARISON OF SIMULATION AND ESTIMATED GALAXY PARAMETERS

Parameter	Simulation derived value (Cygnus A)	Estimate (model and object dependent)	Author
Glactic current, I_z, A	2.15×10^{19}	10^{17}–10^{19}	Alfvén
Galactic magnetic field, B, G	2.5×10^{-4} (B_0) 2.0×10^{-4} (B_{z0})	10^{-5} 3.16×10^{-4} 3.00×10^{-4} 1.20×10^{-4} 10^{-5}–10^{-3}	Perley *et al.* (1979) Mills and Sturrock (1970) de Young and Axford (1967) Hargrave and Ryle (1974) Perola (1981)
Thermal plasma temperature, T_i, keV	2.8	1–10 10	Miley (1980) Gisler and Miley (1979)
Plasma density, n_e, cm^{-3}	1.79×10^{-3}	4×10^{-3}–2×10^{-2} 10^{-4}–10^{-3} 0.6×10^{-3}	Perley *et al.* (1979) Miley (1980) Gisler and Miley (1979)
Density of synchrotron emitting electrons, n_e^{syn}, cm^{-3}	6.9×10^{-9}	10^{-9} 1.5×10^{-8}	Shklovsky (1960) Ginzburg and Syrovatskii (1965)
P_{syn}, ergs s^{-1}	6.2×10^{43} (burst average) 8.1×10^{43} (classical formula)	1.6×10^{44} 4.4×10^{44}	Moffet (1975) Shklovsky (1960)
t_{syn}, yr	8.00×10^{6}	10^{4}–4×10^{6} $> 3 \times 10^{7}$ 5×10^{6}	Sturrock and Barnes (1972) de Young and Axford (1967) Ryle and Windram (1968)
Total source energy, ergs	6.30×10^{62}	10^{64} 10^{57}–10^{61} (minimum)	Sturrock and Barnes (1972) de Young and Axford (1967)
Average energy per electron, T_j, MeV	218	> 100 158	Perola (1981) Sturrock (1969)

To scale the simulation spatial and temporal dimensions, $\Delta = 4\lambda_D = 2.97 \times 10^4$ m and $dt = (4\omega_p)^{-1} = 1.04 \times 10^{-4}$ s, to Cygnus A requires a size/time multiplication factor of $\alpha = 5.6 \times 10^{15}$. For this scaling, conservation of the speed of light dictates that

$$\frac{cdt}{\Delta} = \frac{cdt'}{\Delta'} = 1 \tag{13}$$

where $\Delta' = \alpha\Delta = 1.66 \times 10^{20}$ m and $dt' = \alpha dt = 5.87 \times 10^{11}$ s are the galactic equivalent cell and time step, respectively. The values of n, T, $\boldsymbol{B}$, and $\boldsymbol{E}$ remain the same regardless of whether the simulations are scaled to Δ and dt or to Δ' and dt'.

One immediate consequence of the rescaling is that, while the dimensionless simulation parameters remain untouched, the resolution is reduced, i.e.,

$$\omega_p dt = \omega_e dt' = 0.25 \tag{14}$$

where $\omega_e = 4.17 \times 10^{-13}$ rad/s is the highest epicyclic frequency resolvable ($T_e = 0.478$ Myr).

Checking the parameter values, the velocity between the hydrogenic plasma filaments at $T = 90$ is (10), $\mathbb{V} = 4.56 \times 10^{-3}$ cells per time step, or $4.56 \times 10^{-3}\ \Delta'/dt' = 1260$ km/s, in satisfactory agreement with the assumed value $v = 1000$ km/s. To traverse a distance of $10\Delta' = 55$ kpc between filaments requires 2192 time steps. An exorbitant amount of computer time would be required to study the complete bulk-force interaction, that involves the twisting of filaments, in a three-dimensional EM code. To economically resolve the slow-time Biot–Savart forces, a time scale compression is made by reducing the mass of the ions $m_i = 16m_e$. For this reduction, $10\Delta'$ should be traversed in $\sqrt{(16/1836)} \times 2192dt' = 205dt'$. The measured simulation traversal time is somewhat longer, $\sim 300dt'$, because of the presence of repulsive forces in the full simulation model (7) that are not included in (10).

C. Formation of Hot Spots in Interacting Filaments

When the attraction between adjacent Bennett-pinched Birkeland filaments reduces their mutual separation to a few filamental radii, the r^{-4} repulsion (7) produces a redistribution of the synchrotron-emitting relativistic electron currents within the filaments. The result of this repulsion is an "edge-brightening" (an increased current density in the form of rings at the outer edges of the filaments) as well as a diametrical displacement of current density, caused by the tendency of Birkeland currents to twist about each other at late time (Paper II). This process is depicted in Fig. 6, that shows contours of the magnetic field energy at the midway cross section of the two filaments. Additionally, this figure graphically illustrates the tendency towards further filamentation as the current tubes are flattened into sheet beams. The cross-sectional regions of dense synchrotron-emitting electron currents are called "hot spots" in analogy to their double radio galaxy counterparts (see Section VI-D).

D. Radiated Power and Isophotal Morphologies of Strong Sources

An estimate of the total power emitted as synchrotron radiation follows directly from the results of Section V. During the radiation "burst era" at $T = 90$, the total energy radiated in the form of electric and magnetic field

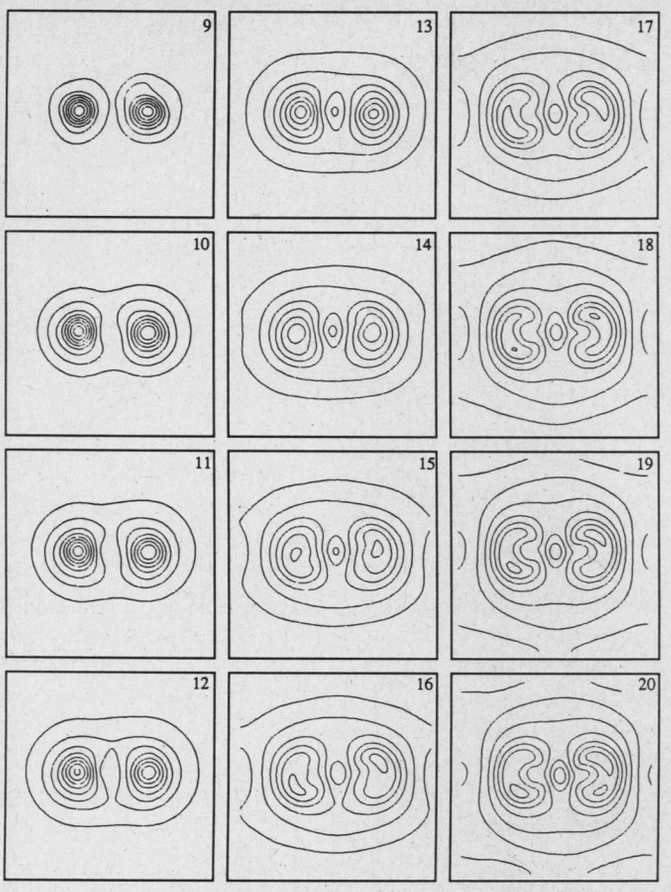

Fig. 6. Contours of magnetic energy B^2 about two adjacent filaments at simulation cross section. T = 9–20 in 1 DT steps. The contours at the location of the two filaments correspond to energy maxima while the central ellipse is an energy minimum. "Hot spots" in azimuthal field energy feeding synchrotron radiation are beginning to become noticeable in the later time frames.

energy is $W_{rad} = 2.1$ AEU while the total simulation magnetostatic energy is $W_{ms} = 350$ AEU. Since, at $T = 90$, $B_z = 2.0 \times 10^{-8}$ T, $B_\theta = 2.5 \times 10^{-8}$ T, and $V \sim 10^{63}$ m^3 is the plasma volume; $W_{ms} = (2\mu_0)^{-1}B^2V = 2.5 \times 10^{53}$ J, or 1 AEU $= 7.1 \times 10^{50}$ J. The peak radiation burst lasts $\sim 20dt'$ in the compressed time frame (Fig. 5), corresponding to an actual time of $20(6 \times 10^{11}\text{ s})\sqrt{(1836/16)} = 1.28 \times 10^{14}$ s. The total power emitted in synchrotron radiation is $L = 2.1 \times 7.1 \times 10^{50}$ J/1.28×10^{14} s $= 1.16 \times 10^{37}$ W, which is to be compared with the radio luminosity of Cygnus A of 1.6–4.4 $\times 10^{37}$ W (Table I).

The synchrotron power derived above is also available from (12). At $T = 90$, the velocity distribution of the Birkeland electrons is nearly Maxwellian with a mean energy of 26.49 keV, or $\beta_z = 0.228$. From (12), $P_{syn} \approx 2.17 \times 10^{-15}B^2n_e\beta^2 = 2.06 \times 10^{-33}$ W/cm^2. The total power or luminosity is then $L = P_{syn}V = 2.06 \times 10^{36}$ W, i.e., about a factor of 6 less than 1.16×10^{37} W resulting from the filament interaction (cf. Fig. 5).

Fig. 7 compares the induced magnetic energy isophotes of the synchrotron-emitting simulation currents to the synchrotron isophotes measured for Cygnus A at a frequency of 150 MHz [72].

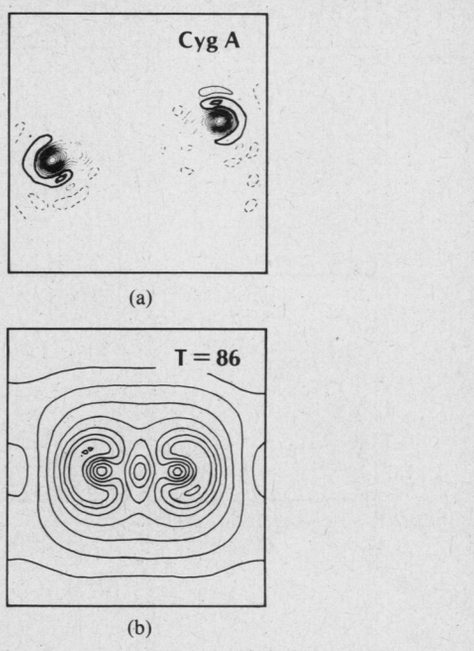

Fig. 7. (a) Isophotal contours of synchrotron radiation at 150 MHz from Cygnus A. (b) Magnetic energy isophotes of filament cross sections near synchrotron burst $T = 86$.

E. Induction Fields

In accordance with Faraday's Law of Induction

$$\nabla \times \boldsymbol{E} = -\partial \boldsymbol{B}/\partial t \tag{15}$$

the converging magnetic fields produce an axially directed induction field E_z, whose strength, based upon a number of frames (time steps) of the cross-sectional view of the simulation magnetic field, can be approximated by

$$E_z \cong -B_\theta \Delta'/dt' \tag{16}$$

or $|E_z| \cong 6.9$ V/m, using the parameters of Section VI-B.

The fully electromagnetic simulation allows the calculation of the induction field from (15) for the more complex magnetic fields B = B(r, θ), and these are shown in Fig. 8. Fig. 8(a) shows the magnetic energy densities $\mathbb{B}^2$ while Fig. 8(b) shows the corresponding electric induction field energy densities $\mathbb{E}^2$. The induction field grows from a value $\mathbb{E}^2 \cong 0.7$ at $T = 104$ to $\mathbb{E}^2 \cong 1.3$ at $T = 300$. In dimensionless simulation units, $\mathbb{E}$ is

$$\mathbb{E} = \frac{c/\omega_p}{mc^2/e}E = \frac{\lambda_E}{W_e}E \tag{17}$$

where $\lambda_E = c/\omega_p$ is the electromagnetic "skin-depth" parameter and $W_e = 511$ keV is the rest mass energy of the electron. In MKS units, the induction electric field corresponding to $\mathbb{E} = 1$ is 3.96 V/m, so that the peak fields E_{z1} at $T = 104$ and 300 are 3.31 V/m and 4.52 V/m, respectively.

F. Temporal Development of Double Radio Sources

During the time that the electromotive force driving the Birkeland currents exists, both axial currents and concom-

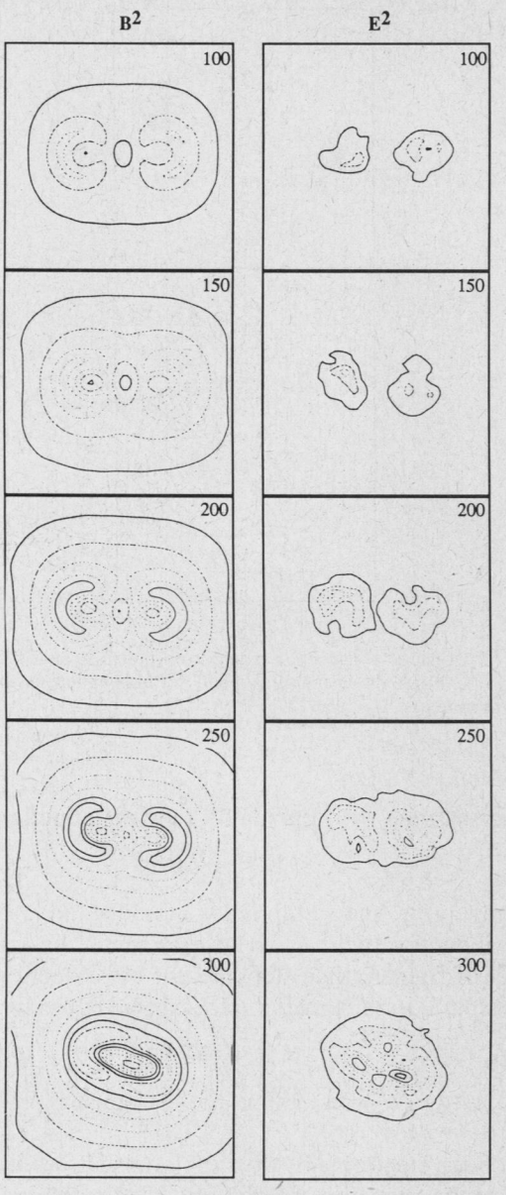

Fig. 8. Electric- (induction) field and magnetic-field energies $\mathbb{E}^2$ and $\mathbb{B}^2$ associated with two interacting Birkeland filaments, T = 100–300 in 50 DT steps. Run TO6.

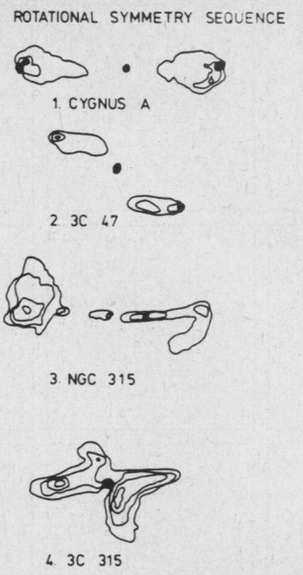

Fig. 9. Rotational symmetry sequence of double radio galaxies (after Miley [65]).

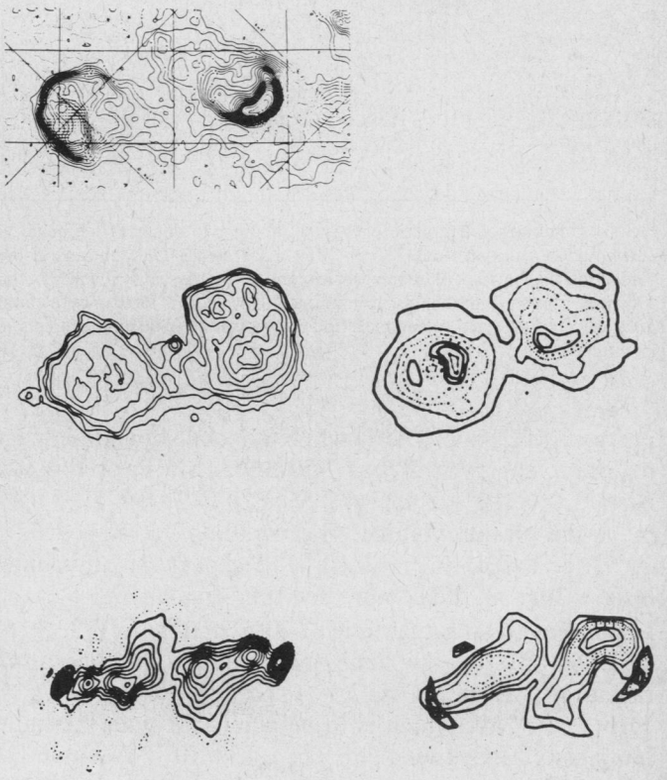

Fig. 10. (a) Isophotes of 3C434.1, Fornax A, and 3C192. (b) Magnetic and electric field energy (composites) simulation analogs.

itant azimuthal magnetic fields increase, producing the distribution of magnetic-field energy shown above (Fig. 8(a)). As previously seen in Fig. 6 ($T \rightarrow$ 1–20), the longer time sequence in Fig. 8 ($T \rightarrow$ 100–300) also shows the tendency toward a rotational displacement in source morphology, from the strong source at T = 90 (peak burst) to the weaker source at T = 300. A suggested sequence in rotational symmetry as a property of double radio sources has, in fact, been noted and is reproduced in Fig. 9.

The approximate age of a double radio galaxy can be determined from its isophotal contour profile at a given wavelength; the isophotes of strong classical double (early) radio galaxies are largely determined by the magnetic energy density of the interacting Birkeland filaments, while (later time) double radio galaxies project more complicated patterns resulting from the induction acceleration of plasma confined between the magnetic isobars. Fig. 10 illustrates this situation by comparing the synchrotron isophotes to the induction electric-field energy patterns for the sources 3C434.1, Fornax A (NGC 1315), and the weaker later time source 3C192 [76].

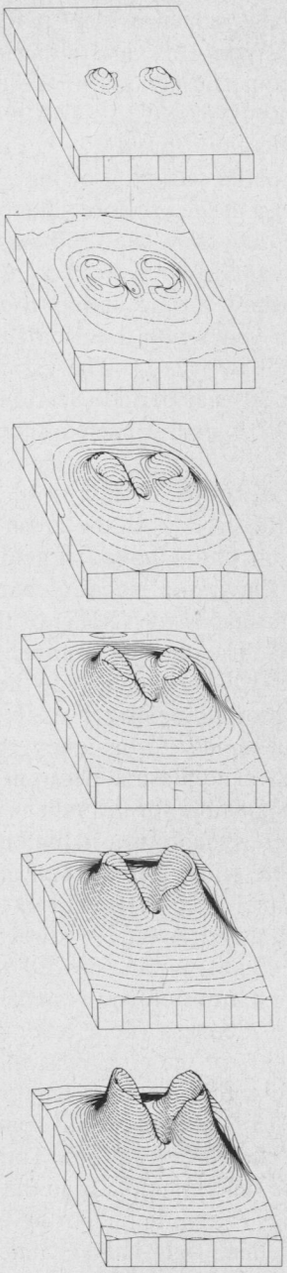

Fig. 11. Development of a double radio galaxy. Isometric view of magnetic energy contours. Time increases from top to bottom.

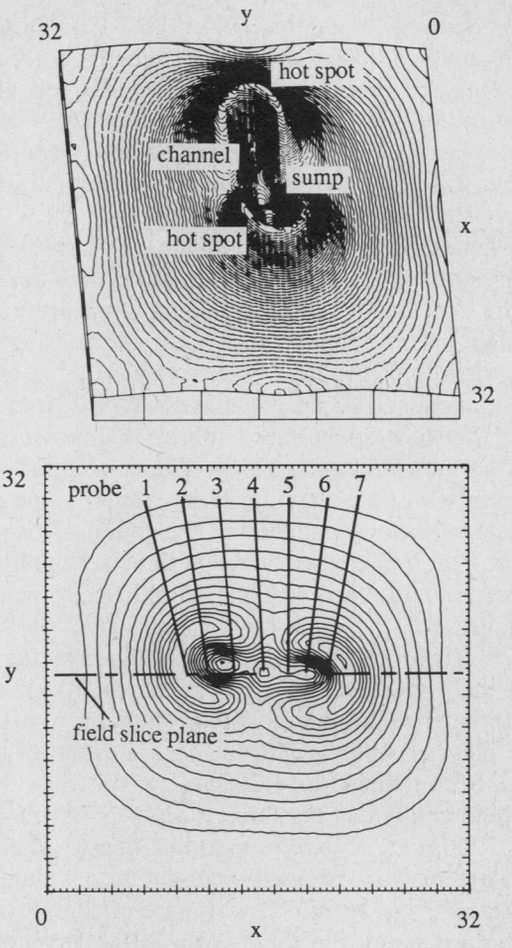

Fig. 12. Isometric and planar views of self-consistent magnetic fields at $T = 255$ showing elliptical sump and one-sided isobaric channel between energy hot spots. Peak field (squared) = 1.5 units, 0.1 units/contour. Simulation run TO6.

VII. The Formation of Elliptical Quasars and Magnetically Confined Sheet Electron Beams (Jets)

A. The Compression of Intergalactic Plasma by Converging Magnetic Mirrors

As the axial currents and concomitant azimuthal magnetic fields about each filament increase, a magnetic isobaric configuration, shown as a function of time in Fig. 11, is produced. The effect of the ''colliding'' magnetic fields is to produce an isobaric sump with elliptical cross section at the separatrix between parallel currents [77]. At $T = 90$, the field strength squared in the vicinity of the sump (approximately midway up on the last frame in Fig. 11) is $\mathbb{B}^2 = 0.2$, or $B_\theta = 0.592 \times 10^{-8}$ T. The field induced pressure defining the boundary of the sump at this time is $p_B = (2\mu_0)^{-1}B_\theta^2 = 1.4 \times 10^{-11}$ Pa (1.4×10^{-10} dyn/cm^2).

At later time, the converging magnetic-field lines continue to compress intergalactic plasma into two narrow channels formed on either side of the elliptical sump. Fig. 12 shows the isobaric contours and isometric veiw at $T = 255$. At this time, a channel exists on the right-hand side of Fig. 12(b), subtended by a 3.8×10^{-11}-Pa (0.98×10^{-8} T) isobar that also encloses the sump. The length of the channel is approximately $9\Delta' = 1.5 \times 10^{21}$ m (49.8 kpc) while the width varies from about $0.5\Delta'$ to $2.0\Delta'$ (2.8–11 kpc).

The condensation of plasma from the cosmic plasma medium involves two mechanisms: the pinching of plasma within the current-conducting filaments, and the capture and compression of plasma between the filaments. The rate of condensation thus depends on whether the plasma is internal or external to a filament.

Within a filament the convection velocity of plasma radially inward is $\boldsymbol{v} = \boldsymbol{E} \times \boldsymbol{B}/B^2$, so that at time $T \sim 100$,

$v_{conv} \sim E_z/B_\theta \sim 60$ mV/m $\div 2 \times 10^{-8}$ T $= 3 \times 10^6$ m/s (3000 km/s), i.e., the convection velocity is three times faster than the Biot–Savart attraction between filaments (the inflow velocity is 30 000 km/s where $B_\theta \sim 2 \times 10^{-9}$ T). Conversely, from Fig. 11, the velocity of a magnetic isobar towards the sump is, approximately, 0.032 cells per time step, or $v_{comp} \sim 0.032\Delta'/dt' = 8.99 \times 10^6$ m/s (8990 km/s), i.e., the approximate velocity of isobaric compression in the region of the sump is nine times faster than the Biot–Savart attraction. It is noteworthy that the incoming plasma closely resembles the closing of two giant cymbals (e.g., Fig. 8(a), frame 3) as is often the case for peculiar galaxies such as NGC 5128 and Cyg A, located between giant radio lobes, that possess "dust lanes" at their midsection [78]. The convection velocity decreases with time, having its maximum value v_{comp} at the onset of plasma convection. The compression velocity increases (as I increases with particle acceleration in a constant E_z field) until pressure equilibrium is reached in the sump.

At $T \sim 100$, the elliptical sump (defined by the boundary of the 1.4×10^{-11}-Pa isobar) extends some 50 kpc and can balance the thermokinetic pressure of a 10^4-m^{-3} 6-keV plasma. At $T = 255$, the spatial extent of this isobar has been reduced to ~ 20 kpc. At this time the magnetic-field gradient at the sump is $\delta B/\Delta' = 0.0554$, or 4.4×10^{-26} G/m (1.32 pG/kpc), so that nearly all of the intergalactic plasma originally present in a volume $V \sim 4/3\ \pi(2.5\Delta')^3 = 3 \times 10^{62}$ m^3 has been compressed into the elliptical sump. For the $2\text{–}2.5 \times 10^{-8}$ T contours, the pressure is 2.5×10^{-9} Pa, allowing the confinement of a 10^9-m^{-3} (10^3-cm^{-3}) 2-eV plasma. (The concentrated plasma at the center of the sump has not yet been modeled because of demands on spatial resolution in a simulation. Lerner has studied this state in some detail and points out the similarity to pinch regions in the dense plasma focus [15].)

The phenomena associated with the capture and compression of intergalactic plasma between neighboring Birkeland currents in synchrotron emission can best be seen from the observational evidence itself (Figs. 13 and 14) [79]–[81]. Fig. 13(a) illustrates double sources for which no central "object" of any kind is present, while Fig. 13(b)–(c) illustrates sources in which large-red-shift QSO's have formed at or near the geometric center between filaments. Fig. 14 shows the isophotes of double sources for which the central object is identified as galactic in nature; usually having a large red shift, and being elliptical or peculiar in morphology. This variety of source represents a later stage in temporal evolution and is accompanied by somewhat richer isophotal patterns because of the action of the inductive field on the confined plasma.

B. Temporal and Spatial Characteristics of the Induction Acceleration Field

A temporal–spatial history of the electric and magnetic fields within the simulation region is possible from field probes and field-slice plots. Fig. 15 shows the temporal history of the axial induction electric field E_z measured at the ordinate position $16\Delta'$ and along the "major axis" between the geometric centers of the Birkeland currents at abscissa points $10.5\Delta'$, $12\Delta'$, $14\Delta'$, $16\Delta'$, $18\Delta'$, $20\Delta'$, and $21\Delta'$, respectively (probes 1–7, Fig. 12(b)). Fig. 16 illustrates the spatial variation of the E_z field component along the abscissa at the ordinate slice position $16\Delta'$. The probe and slice data show the following.

1. Variability in Synchrotron Flux: The temporal probe data (Fig. 15) show a time variation $d\mathbb{E}/dt' \sim 0.75/dt'$ (14.6 μV/m per year) with a periodicity $\sim 5dt'$ (i.e., an expanded time $\sim 10^6$ years). The variability is appreciable even over a 30-year period (Section VII-C), i.e., 438 mV/m, or $\sim 10^{16}$ V over a parsec-dimensioned acceleration length.

2. One-Sidedness in Synchrotron Radiation [82], [83]: Fig. 16 illustrates both the gross channel morphology and slice plots of the induction fields at selected times of Fig. 15. As shown, an isobaric channel has started to form on the right-hand side (RHS) of the sump, or core, at time $T \sim 193$. The channel continues to form and narrow until $T \sim 243$, when a change in the converging magnetic-field line morphologies ceases to support a channel on the RHS, but rapidly forms a new channel of the left-hand side (LHS). The plasma electrons confined in these channels are responsible for the synchrotron radiation observed. However, synchrotron radiation from the channel plasma is possible only when the polarity of the induction field in the channel is correct. (For example, the electric field must be directed in the $-z$ direction (inward from the plane of the figure) for an outward observation of synchrotron radiation from electrons accelerating in the $+z$ direction.) One-sidedness (field reversal or a large field ratio on either side of the core) was measured by probes 5 and 6 (located within the right-hand channel) for $T \sim 190\text{–}290$ (Fig. 15; the actual field spatial profiles at selected times are shown in Fig. 16). Thus at time $T = 255$ (Fig. 12(b)), the field component in the left-hand channel is directed along $+z$, while the strong-field component in the more well-defined right-hand channel is directed along $-z$. Thus this source projects a channel or "jet-like" radiation pattern in the $+z$ direction that is connected to a strong core ($P \propto E_z^2$). This is also the direction in which the synchrotron radiation from the electron Birkeland currents making up the outer radio lobes is beamed.

3. Electric and Magnetic Field Configuration: During the synchrotron burst era $25 \leq T \leq 140$ the plasma being collected within the core and channels is tenuous. The induction field is positive on both sides of the core but, at times, the left and right components can differ appreciably in magnitude by a ratio as high as 5 : 1. This era also corresponds to a weak core field and magnetic fields that are largely transverse to the major axis. A transition from transverse to parallel magnetic fields is observed at about $T = 190$. As shown in Fig. 16, the $B_\parallel$ channels become increasingly "collimated" for $T > 200$ and are accompanied by an increasing core field when $250 \leq T \leq 360$ (Fig. 15, probe 4).

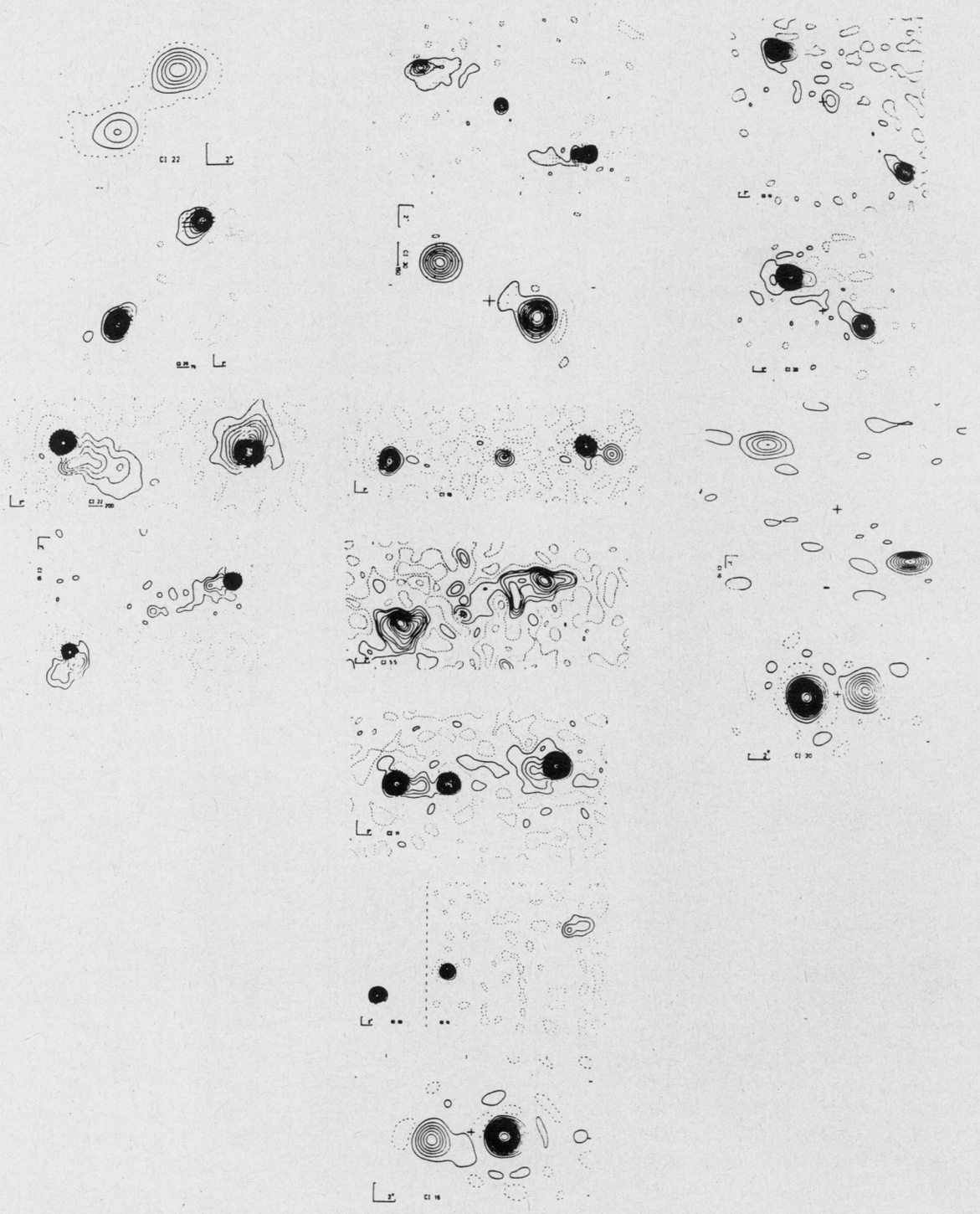

(a) (b) (c)

Fig. 13. Fifteen QSO's with and without an optically identifiable object between radio lobes. (a) 3C86B, 3C427.1, 3C86A, 3C69. (b) 3C47, 3C194, 3C204, 3C215, 3C249.1, 3C263, 3C288.1. (c) 3C323.1, 3C336, 4C28, 3C18. All measurements taken at 5 GHz.

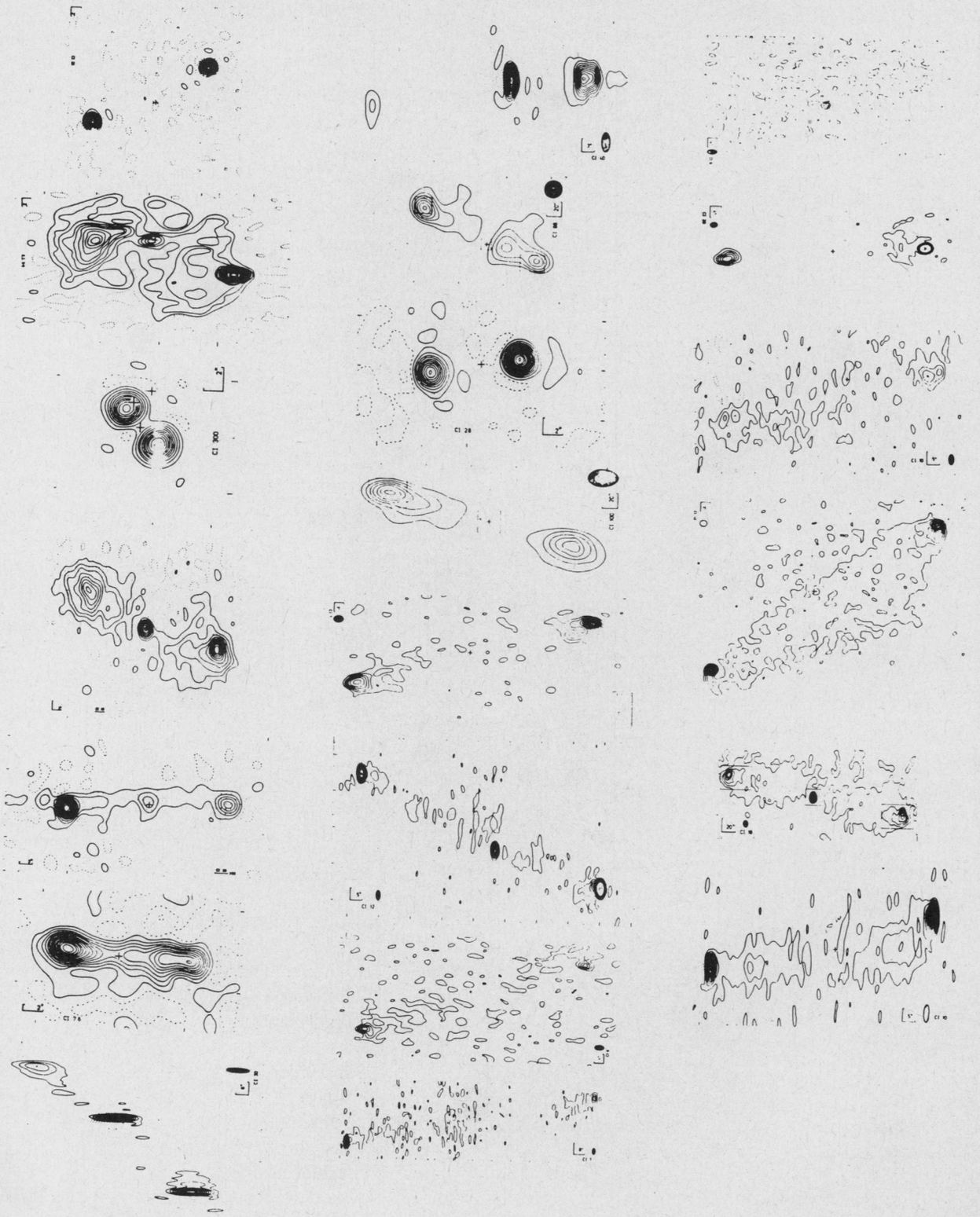

(a) (b) (c)

Fig. 14. Twenty-one QSO's having a galactic object situated midway between radio lobes. (a) 3C61, 3C277.3, 3C295, 3C388, 3C411, 3C434, 3C190. (b) 3C154, 3C184, 3C171, 3C223, 3C234, 3C298.2, 3C284. (c) 3C332, 3C381, 3C357, 3C430, 3C456, 3C79.

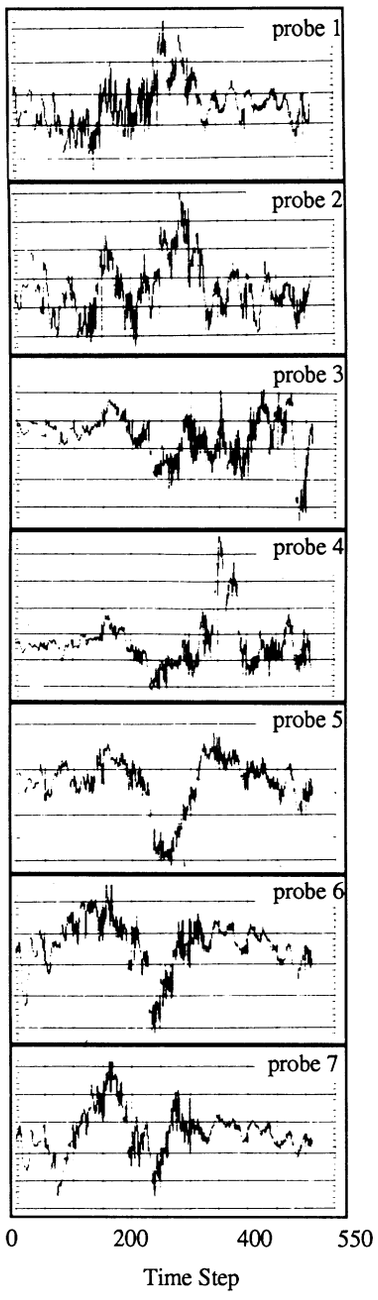

Fig. 15. Electric field E_Z versus time at probe positions 1-7 (Fig. 12). The ordinate is given in simulation units. Calibration: 1 unit/div (probe 5, 2 units/div). Zero field, first line, probes 1, 2, and 4; second line, probes 3, 5, 6, 7. Run TD6.

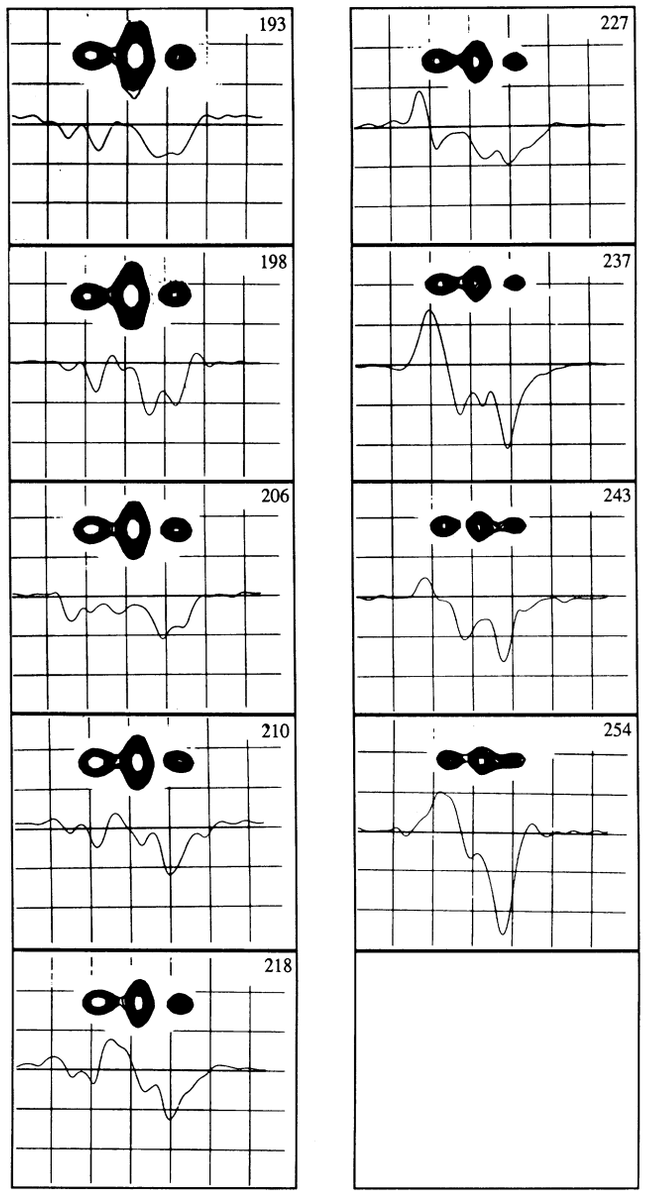

Fig. 16. Spatial slice plots of E_Z (spectral brightness $\approx E_Z^2$) along source major axis at selected time T = 193, 198, 206, 210, 218, 227, 237, 243, and 254. Ordinate, 2 simulation units/div. Abscissa, 0-35 Δ'. Insets illustrate the magnetic isobaric profile at time step.

The total intensity along a source observed at radio and microwave wavelengths must be determined by the square of the induction field within the source. Fig. 17 depicts the total intensity distribution of the radio galaxy 3C326 on a crosscut along its major axis at 49 cm. The intensity profile recorded corresponds approximately to that measured in the simulation at $T \sim 206$ in Fig. 16 (cf. [84]). Knowledge of the field strengths and plasma density allows a quantitative analysis of the brightness of plasma within the channels, and can be directly compared to data [85], [86]. These comparisons are not made in this paper.

4. Polarization: Plots of the angular distribution of radiation from mildly relativistic electrons, 1–200 keV, are given by Oster [87]. For frequencies above the second electron cyclotron harmonic, the radiation pattern of each filament is largely polarized in the x–y plane (cf. Figs. 5 and 18).

5. Superluminosity: The rapid spatial variation of the induction field, as well as the changing of the field polarity along the channel, causes an apparent "superluminosity" effect as the field sweeps the channel confined plasma. Superluminosities are often associated with radio sources [88] and apparent "superluminosities" as high as seven times the speed of light have been measured in the simulation. (The decrease in the induction field strength because of a reduction in the rate of change of the magnetic field along the channel does not require a high degree of alignment of the source with the observer. Moreover, while $7c$ is the highest phase velocity seen in the simulations, there is no reason why phase velocities cannot be appreciably higher than this value.) The electro-

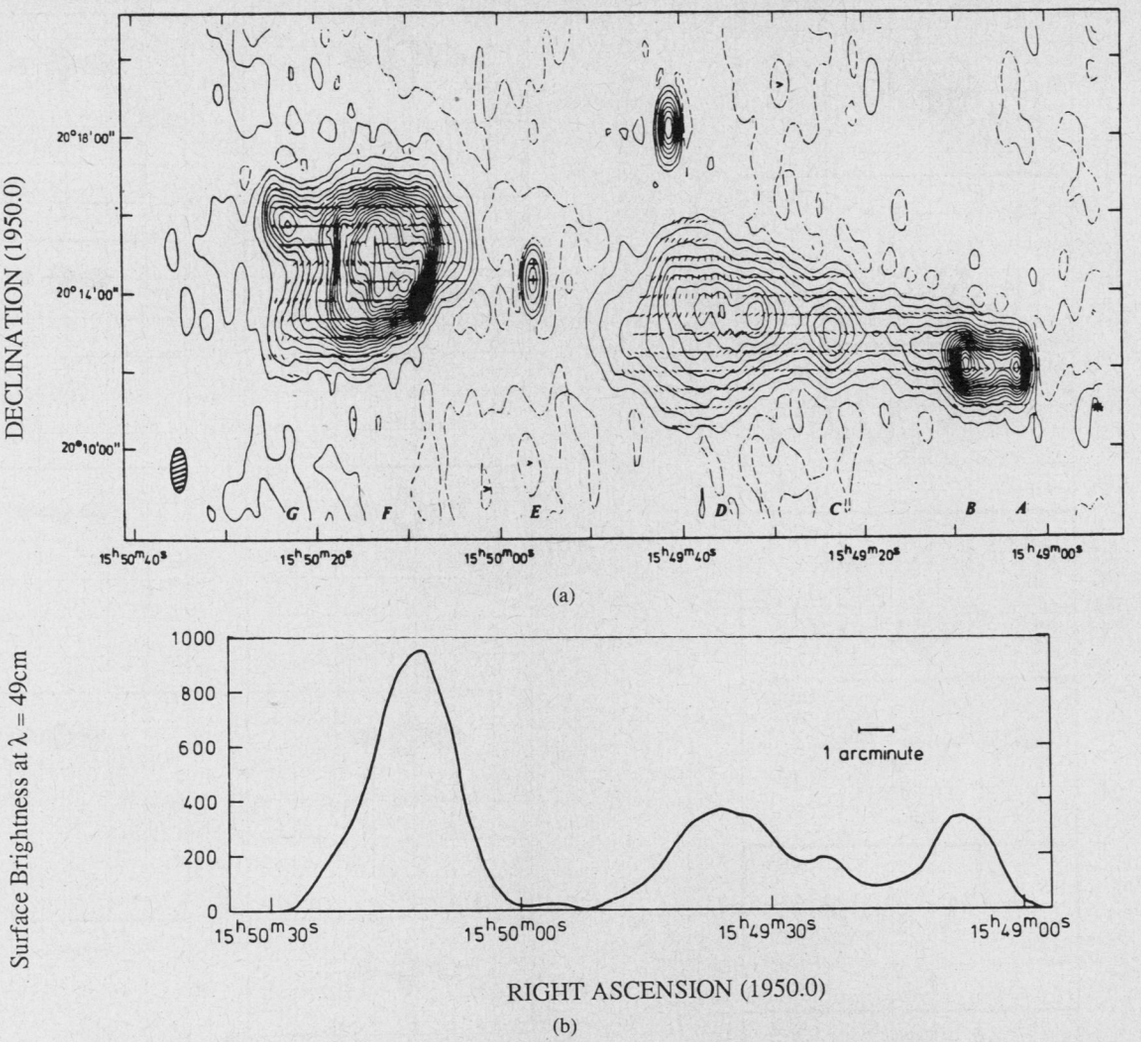

Fig. 17. (a) Westerbork 21-cm map of the radio galaxy 3C 326 on which are superimposed vectors indicating the orientation of the magnetic field projected perpendicular to the line of sight. (b) A crosscut along the major axis of 3C 326 showing the 49-cm spectral index distribution of the outer lobes (after Willis [84]).

magnetic wave effect for illumination as a source of "superluminosity" was first suggested by Kellerman [89]. Isophotal contour maps and major-axis profile data measured from quasars can be directly compared to the simulation data in Fig. 16 [90]. The ignition of previously confined plasma is also demonstrated by nonradial appearances of the isobaric profiles taken on by the plasma [91]. These profiles are not seen in side-on observations of charged particle beams, but are observable when a sheet beam is viewed end-on.

C. Simulating the Induction Accelerated Sheet Beam

For the purpose of resolving the plasma magnetically confined within the 5 × 50-kpc channel, a simulation with a temporal/spatial resolution increased approximately two and one-half times is used. The channel length and width are $24\Delta''$ and $5\Delta''$, respectively, where $\Delta'' = 6.25 \times 10^{19}$ m. The time step is $dt'' = 2 \times 10^{11}$ s. To insure that all the particles simulated are magnetically confined, the 10^{-13}-Pa thermokinetic isobar is chosen to define the

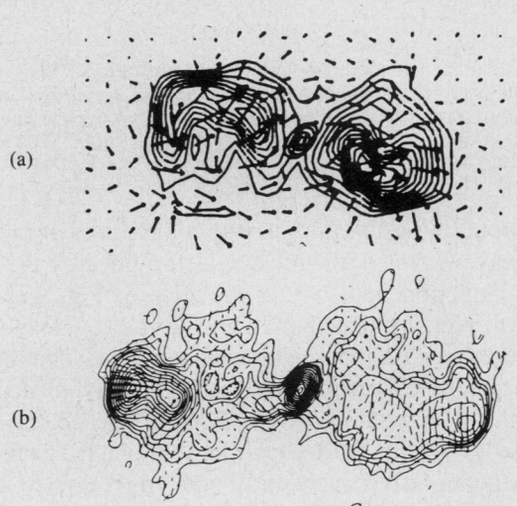

Fig. 18. (a) Electric energy and magnetic elliptical sump at $T = 237$ in simulation run TO6. The arrows denote the magnetic-field polarization vectors in this synchrotron source. (b) Isophotal contours of the source 2355 + 490. The arrows indicate the orientation of the magnetic field projected perpendicular to the line of sight.

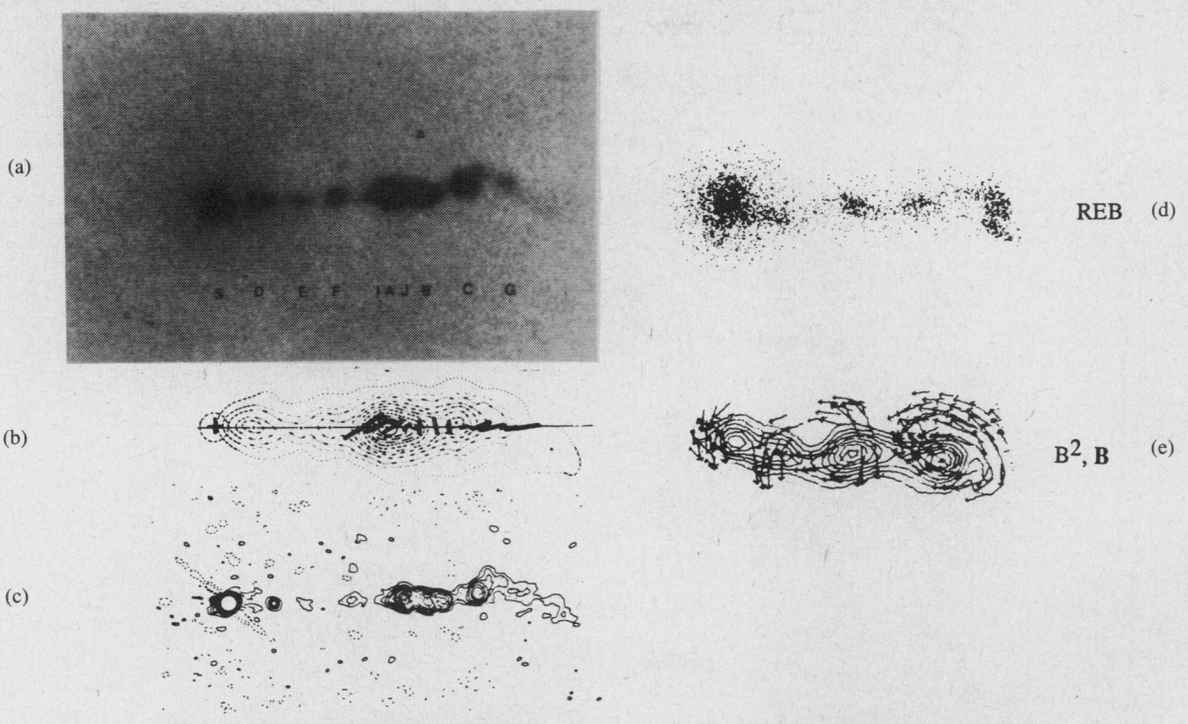

Fig. 19. (a) Optical synchrotron radiation from the jet (sheet beam) in M87. (b) Isophotes and projected magnetic field vectors. (c) Vortex filaments within jet. (d) Relativistic electrons in jet simulation (the sheet beam electrons trapped within the magnetic isobaric channel are inductively accelerated out of the plane of the figure and not sideways to the right). (e) Magnetic energy contours and polarization vectors from simulation.

channel dimensions. (Because of the steepness of the isobars, this dimension is practically the same as that subtended by the 10^{-11} isobar.) Based on this pressure, suitable choices for the electron density and temperature are 2×10^3 m^3 and 300 eV, respectively. A spatially averaged induction field $E_z \sim 600$ mV/m is used. The dimensionless simulation units are $\omega_p dt = 0.25$, $\lambda_D/\Delta = 0.1$, and $\omega_{c0}/\omega_p = 5.0$, and the scaling factor is $\alpha'' = 2.1 \times 10^{15}$. The number of electrons per cubic cell is 10.

Because of the $\boldsymbol{E}_r \times \boldsymbol{B}_{z0}$ diocotron instability, sheet beams filament into current bundles whenever a threshold determined by the length of propagation or current carried by the beam is exceeded [26]. The quantity $\boldsymbol{E}_r$ is the spatially dependent electric field across the sheet width in a nonneutral beam (or in an overall neutral beam when the $\boldsymbol{B} \times \nabla B$ force produces charge separation). This phenomenon was first discussed by Alfvén in connection with charge bundles and folds in the context of auroras [92]. The optical synchrotron radiation, isophotes, and vortex filaments of the jet (sheet beam) in M87 are depicted in Fig. 19(a)–(c). Fig. 19(d) shows the filamentation within the simulation sheet beam. Also shown are the magnetic-field contours $\mathbb{B}^2$ and the $\boldsymbol{B}$-field-polarization vectors. As shown in Fig. 19, the LHS of the beam is tethered to the denser core, but the RHS is free to fold (within the constraints determined by the strength of the external magnetic pressure). The configuration shown is typical of sources such as M87 and 3C273 [93]–[102]. The polarization of the self-consistent magnetic field is also shown in Fig. 19(e) and is in agreement with measured polarization data [103]–[107].

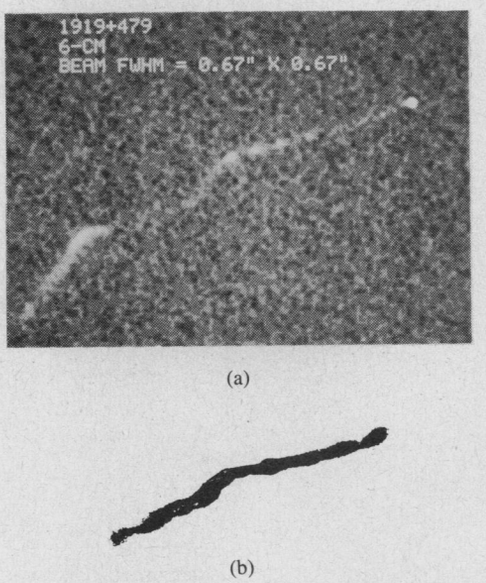

Fig. 20. (a) The jet in 1919 + 479. (b) Laboratory sheet beam at early time (after Peratt [39]).

Fig. 20 illustrates the filamentation within the extragalactic source 1919 + 479 at 6 cm, shown together with its laboratory analog. The bends in sheet beams, either extragalactic or laboratory, delineate where the dynamics of the beam change from that of a (linear) rigid rotor to a (nonlinear) vortexing beam. Typically, this change occurs

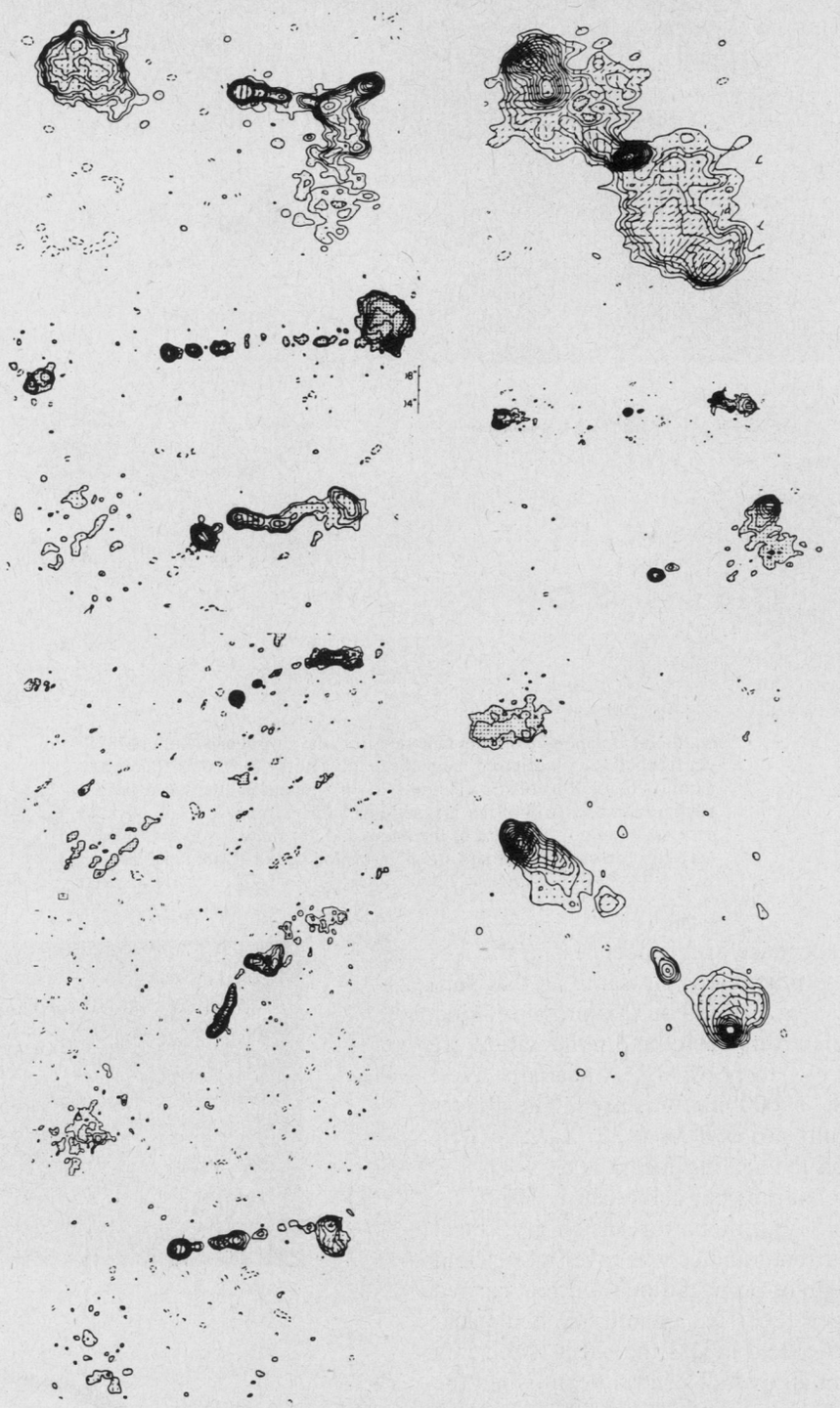

Fig. 21. Ten examples of very large array observations of radio quasars having jets [115]. The general morphology is that of a filamented structure in emission that is connected to a core located midway between two strong radio emitting plasmas. The last three pictures are designated as "faint" jets.

when the beam has rotated some 10°–30° about the major axis, depending again on the "collimation" pressure of the external magnetic isobars. It is emphasized that the sheet beam is produced between the converging isobars and is inductively accelerated out of (or into) the plane of the figure.

D. Discussion

The term "jet" was first used in astrophysics by Curtis in 1918 to describe the elongated optical feature protruding from the core of the elliptical galaxy M87 [108], [109]. Later Baade and Minkowski suggested that such a

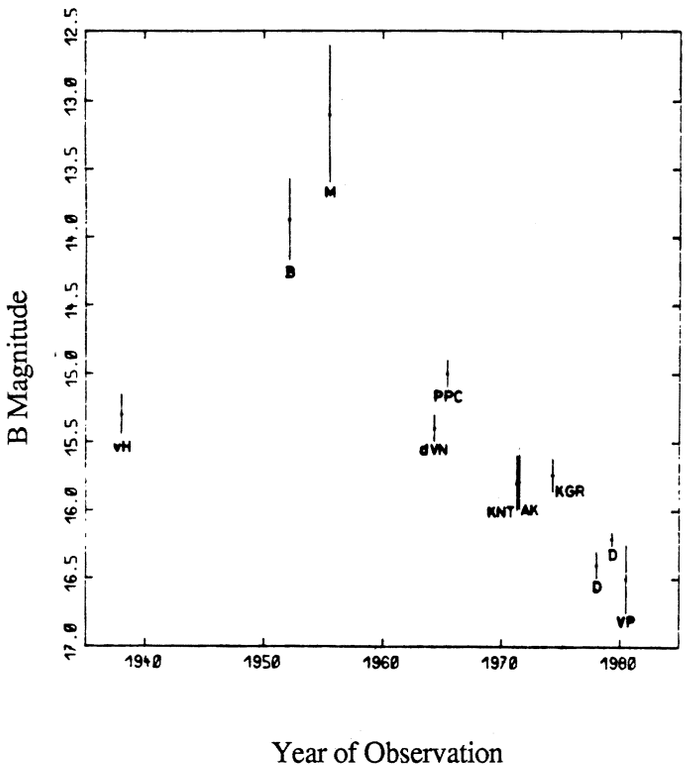

Fig. 22. Independent estimates of the magnitude of the jet of M87 in the *B* waveband plotted according to date of observation (after Warren-Smith *et al.* [116]).

jet might actually correspond to matter ejection after some active phase of the core [110]. Jets have been mapped in about 200 radio sources. Jets are found not only in double radio galaxies and quasars, but also in central compact radio sources located in the nucleus of associated (optical) galaxies (Paper II) [111]–[113]. They are measured from the electromagnetic (synchrotron) radiation they emit, from centimeter wavelengths to X rays. However, in spite of improved resolution and statistics of observations, definitive direct evidence that ordered streaming motions are present in jets or radiosources is still missing. Moreover, uncertainty exists in identifying structures as either "jets" or "bridges" [114].

Fig. 21 shows VLA observations of radio quasars having jets (seven out of 26 quasars in a 966-MHz Jodrell Bank survey) and three quasars with faint jets [115]. The general morphology is that of a filamented structure in emission (see Section V-B) that is connected to a core (see Sections VII-A and -B) located midway between two strong radio plasma sources. These data are consistent with Fig. 16, which indicates that the source geometry can consist of a core and channel (that may be filamented and bent) or a core with a side node. The topology mapped is dependent on the polarity of the induction field and the direction of observation.

Lastly, as indicated in Section VII-B1, the induction field across the channel is variable, causing the preconfined plasma to brighten or fade. Fig. 22 shows the magnitude of the optical synchrotron radiation from M87 and its filamented channel versus observed time [116]. Comparison of the integrated magnitude of the jet with previous independent measurements over the period 1934–1980 suggests that the jet is variable and has been fading more or less uniformly by about 0.8 mag per decade between 1964 and 1980. The data imply that over the period 1952–1980, the total jet intensity fell by at least 2.5 mag. Comparisons of isophotes taken in 1964 and 1979 show no obvious differences in overall shape, apart from effects of variation and noise. This indicates that the fading has affected the whole channel more or less uniformly since 1964, i.e., the knots (i.e., filaments or vortices) have not been seen to move. However, between 1934 and 1956, knots *A* and *B* became significantly brighter than *C*.

At a distance of 11.4 Mpc, the channel length of M87 is 30 arcsec in the plane of the sky, or 5400 light years across. For this reason, and because side-on photographs of charged-particle beams display different morphologies, the explanation of observable jet fading based on side-ejected matter models is untenable. However, the morphology, field configuration, polarization, and variability of M87 are in agreement with laboratory and simulation analogs of outwardly propagating sheet jets.

VIII. Discussion

In discussing the Biot–Savart forces between adjacent circuit currents a problem arises: Ampere's problem, i.e., the necessity of accounting for the complete electrical circuits in which the currents flow. This problem applies to cosmic as well as laboratory plasmas. Unlike the previous sections, where the specification of a single physical quantity was sufficient to scale all parameters in the simulation study of double radio galaxies, the discussion of the entire circuit is far more speculative since this is not modeled. (Particle codes have, in fact, advanced to a level where an external circuit consisting of lumped circuit elements can be included in the simulation.) Nevertheless, based upon the properties of plasma in the laboratory, a reasonable guess about the properties of the cosmic circuit is possible.

In its simplest form, an electrical circuit consists of a voltage source, a load, and the transmission line between the source and load. For the case studied here, the transmission line and the load are the field-aligned current that is likely to form (a series of) double layers. Like most field-aligned currents in cosmical plasma, the currents flowing from the source to the double layers are likely to be pinched. This means that they consist of filaments [16], [117]. The magnetic field is of the order $B = \mu_0 I/2\pi r$, where r is the radius of the filament or bunch of filaments. In circuit theory the magnetic energy of the circuit is described as being due to an inductance L, such that

$$\tfrac{1}{2} LI^2 = \int \frac{B^2}{2\mu_0}\, dV \qquad (18)$$

where I is the current. The integral should be taken over the whole region where I produces a magnetic field.

Since the circuit conducts filamentary currents, the circuit consists of a resistance, an inductance, and electrostatic double layers formed along the filaments, all fed by an EMF. The circuit equation is

$$L\frac{dI}{dt} + RI = V_{\text{source}} - \sum V_{\text{DL}} \tag{19}$$

where ΣV_{DL} is the sum of the potentials over the double layers, and R and L are the resistance and inductance of the circuit, respectively.

If R is negligible (as is often the case in cosmic situations) the current grows as long as $V_{\text{source}} > \Sigma V_{\text{DL}}$. If $\Sigma V_{\text{DL}} = V_{\text{source}}$, the current is constant. For the simulated pair of Birkeland filaments (Section VI-D), $\frac{1}{2}LI^2 = 2.5 \times 10^{53}$ J and $I = 2.15 \times 10^{19}$ A; so that $L = 1.08 \times 10^{15}$ H. The rate of increase of the current is $\Delta I/\Delta t = 2.15 \times 10^{19}$ A/90 $dt' = 3.98 \times 10^5$ A/s. For these values, $LdI/dt = 4.2 \times 10^{20}$ V.

In analogy to the rotating magnetized plasma dynamos that drive cosmic Birkeland currents of lesser dimension, a magnetized plasma with a size of the order of the largest objects observed in the universe, 10–50 Mpc, moving through 10^{-9}-T field lines at 1000 km/s, will produce an EMF of the order of 10^{20} V. Using Cygnus-A-dimensioned current cross sections, 35 kpc, and the knowledge that the width/length ratio of laboratory filaments is generally in a range 10^{-3}–10^{-5}, a typical filament length associated with the dynamo source may be of the order of 350 Mpc.

If suddenly V_{source} becomes zero, the current will continue to flow but it will decrease with the time constant $T_c = LI/\Delta V \approx 10^{14}$ s.

IX. Conclusions

Because of *in-situ* measurements of plasmas in Earth's ionosphere, cometary plasmas, and the planetary magnetospheres and recent discoveries of helical and filamentary plasma structures in the Galaxy and in extragalactic objects, our understanding of cosmic plasma has changed considerably during the last decade. In particular, Birkeland (field-aligned) currents, double layers, and field-aligned electric fields are now known to play a far more important role in the evolution of plasma in space, including the acceleration of charged particles to high energies. Because the properties of the plasmas in space are found to differ little from those in the laboratory, the empirical knowledge gained from earth-bound experiments has suddenly found application in situations orders of magnitude greater in dimension. Kirchhoff's laws for currents in circuits appear equally valid regardless of whether the plasma has its dimensions measured in centimeters, kilometers, parsecs, kiloparsecs, or megaparsecs.

With the advent of three-dimensional electromagnetic particle-in-cell simulations, investigations of Birkeland currents, double layers, and field-aligned electric fields have become possible in plasmas not accessible to *in-situ* measurement, i.e., in plasmas having the dimensions of galaxies or systems of galaxies. The necessity for a three-dimensional electromagnetic approach derives from the fact that the evolution of magnetized plasmas involves complex geometries, intense self-fields, nonlinearities, and explicit time dependence. Moreover, synchrotron radiation and double layers are discrete particle phenomena and cannot be studied using magnetofluid models of plasma. The importance of applying electromagnetism and plasma physics to the problem of radio galaxy, galaxy, and star formation derives from the fact that the universe is largely matter in its plasma state, i.e., a *plasma universe*. The motion of this plasma in local regions can lead to pinches and ultimately condense states of matter. Where double layers form in the pinches, strong electric fields can accelerate the charged particles to high energies. Simulations of the interactions between plasma pinched into filaments show:

1) a burst of synchrotron radiation of luminosity $\sim 10^{37}$ W lasting 10^7–10^8 years as the interaction begins;
2) isophotal topologies of double radio galaxies and quasars, including juxtaposed "hot spots" in the radio lobes (cross sections of the interacting Birkeland currents);
3) the formation of "dust-lane" peculiar and elliptical galaxies at the geometric center of quasars and radio galaxies (due to plasma trapped and compressed within the elliptical magnetic separatrix);
4) a spatially varying power law along the major axis of the simulated double radio galaxies in agreement with observations;
5) alternating beams of betatron pumped synchrotron-emitting electrons on either side of the elliptical center. These have the morphologies (i.e., "knots" or vortices) and polarization properties of jets but are aligned in an acceleration direction toward the observer; and
6) a "superluminosity" and fading of jets as the betatron induced acceleration field sweeps over and ignites previously confined plasma.

The simulation time frame of this investigation lasted some 10^8–10^9 years. The lifetime and evolution of quasars and double radio sources, the so-called end problem of double radio galaxies, is addressed in a sequel paper (Paper II) by continuing the simulation run ~ 1–5×10^9 years farther in time. Above all, a translation of knowledge between laboratory, space, and cosmic plasma is indicated from the results outlined above.

References

[1] H. Alfvén, *Cosmic Plasma*. Dordrecht, Holland: Reidel, 1981.
[2] H. Alfvén, "Paradigm transition in cosmic plasma physics," *Physica Scripta*, vol. T2/1, pp. 10–19, 1982.
[3] H. Alfvén, "Paradigm transition in cosmic plasma physics," *Geophys. Res. Lett.*, vol. 10, pp. 487–488, 1983.
[4] L. P. Block, "Double layers in the laboratory and above the aurora," in *Physics of Auroral Arc Formation* (Geophysical Monograph Series, vol. 25). Washington, DC: Amer. Geophys. Union, 1981, pp. 218–225.

[5] P. Carlqvist, "On the formation of double layers in plasma," *Cosmic Electrodyn.*, vol. 3, pp. 377-388, 1972.
[6] L. P. Block, "A double layer review," *Astrophys. Space Sci.*, vol. 55, pp. 59-83, 1978.
[7] C.-G. Fälthammar, "Non-resistive electric drops in cosmical plasmas," in *Particle Acceleration Mechanisms in Astrophysics*, J. Arons, C. McKee, and C. Max, Eds. New York: Amer. Inst. of Physics, 1979, pp. 27-41.
[8] H. Alfvén, "Electric currents in cosmic plasma," *Rev. Geophys. Space Phys.*, vol. 15, pp. 271-284, 1977.
[9] H. Alfvén, "Model of the plasma universe," *IEEE Trans. Plasma Sci.*, vol. PS-14, no. 6, pp. 629-638, Dec. 1986.
[10] P. A. Sturrock, "A model of quasi-stellar radio sources," *Nature*, vol. 211, pp. 697-700, 1966.
[11] P. A. Sturrock and C. Barnes, "Activity in galaxies and quasars," *Astrophys. J.*, vol. 176, pp. 31-45, 1972.
[12] H. Alfvén, "Double radio sources and the new approach to cosmic plasma physics," *Astrophys. Space Sci.*, vol. 54, pp. 279-292, 1978.
[13] A. L. Peratt and J. C. Green, "On the evolution of interacting magnetized galactic plasmas," *Astrophys. Space Sci.*, vol. 91, pp. 19-33, 1983.
[14] P. F. Browne, "Magnetic vortex tubes, jets and nonthermal sources," *Astron. Astrophys.*, vol. 144, pp. 298-314, 1985.
[15] E. J. Lerner, "Magnetic self-compression in laboratory plasmas, quasars and radio galaxies, Part I," *Lasers and Particle Beams*, vol. 4, part 2, pp. 193-222, 1986.
[16] W. H. Bostick *The Cosmology and Morphology of the Electron, Photon, and Other Elementary Onta*, chap. 3, to be published.
W. H. Bostick, "The electromagnetic ram action of the plasma focus as a paradigm for the generation of cosmic rays and the gigantic jets in active galaxies," in *Proc. Tenth Int. Cosmic Ray Conf.*, OG Sessions (La Jolla, CA), vol. 3, 1985, p. 18.
[17] S.-I. Akasofu, "The magnetospheric currents: An introduction to magnetospheric currents," in *Magnetospheric Currents*, T. A. Potemra, Ed. (Geophysical Monograph No. 28). Washington, DC: Amer. Geophys. Union, 1984, pp. 29-48.
[18] W. J. Hiekkila, "Magnetospheric topology of fields and currents," in *Magnetospheric Currents*, T. A. Potemra, Ed. (Geophysical Monograph No. 28). Washington, DC: Amer. Geophys. Union, 1984, pp. 208-222.
[19] H. Alfvén, "Space plasma—The fourth state of matter," *Johns Hopkins APL Tech. Digest*, vol. 6, pp. 100-102, 1985.
[20] A. Dessler, "Evolution of arguments regarding existence of field aligned currents," in *Magnetospheric Currents*, T. A. Potemra, Ed. (Geophysical Monograph No. 28). Amer. Geophys. Union, 1984.
[21] T. W. Hill, "Rotationally-induced Birkeland current systems," in *Magnetospheric Currents*, T. A. Potemra, Ed. (Geophysical Monograph No. 28). Washington, DC: Amer. Geophys. Union, 1984, pp. 340-349.
[22] C.-G. Fälthammar, "Magnetosphere-ionosphere coupling," in *Proc. ESA Workshop on Future Missions in Solar, Heliospheric, and Space Plasma Physics* (Garmisch-Partenkirchen, Germany), Apr. 30-May 3, 1985, pp. 107-133.
[23] V. Nardi, W. H. Bostick, J. Feugeas, and W. Prior, "Internal structure of electron beam filaments," *Phys. Rev. A*, vol. 27, pp. 2211-2217, 1980.
V. Nardi, in *Proc. Second Int. Conf. on Energy Storage, Compression, and Switching* (Venice, Italy, 1978). New York: Plenum, 1982.
[24] B. Lehnert, "An instability of laminar flow of mercury caused by an external magnetic field," *Proc. Roy. Soc. A*, vol. 233, pp. 299-302, 1955.
[25] A. L. Peratt and P. Koert, "Pulsed electromagnetic acceleration of exploded wire plasmas," *J. Appl. Phys.*, vol. 54, pp. 6292-6301, 1983.
[26] A. L. Peratt and C. M. Snell, "Microwave generation from filamentation and vortex formation within magnetically confined electrons beams," *Phys. Rev. Lett.*, vol. 54, pp. 1167-1170, 1985.
[27] H. F. Webster and T. J. Hallinan, "Instabilities in charge sheets and current sheets and their possible occurrence in the aurora," *Radio Sci.*, vol. 8, pp. 475-482, 1973.
[28] D. A. Mendis, "On the hydromagnetic model of comets," *The Moon and the Planets*, vol. 19, pp. 361-369, 1978.
[29] F. Yusef-Zudeh, M. Morris, and D. Chance, "Large, highly organized radio structures near the galactic centre," *Nature*, vol. 310, pp. 557-561, 1984.
[30] R. A. Perley, J. W. Dreher, and J. J. Cowan, "The jet and filaments in Cygnus A," *Astrophys. J.*, vol. 285, pp. L35-L38, 1984.
[31] C.-G. Fälthammar, "Generation mechanisms for magnetic-field-aligned electric fields in the magnetosphere," *J. Geomagn. Geoelectr.*, vol. 30, pp. 419-434, 1978.
[32] C.-G. Fälthammar, "Magnetic-field-aligned electric fields," *ESA J.*, vol. 7, pp. 385-401, 1983.
[33] C. Chan and N. Hershkovitz, "Transition from single to multiple double layers," *Phys. Fluids*, vol. 25, pp. 2135-2137, 1982.
[34] A. L. Peratt and M. E. Jones, "Particle-in-cell simulations of heavy ion plasma double layers," presented at *IEEE Int. Conf. Plasma Sci.*, Saskatoon, Canada, 1986.
[35] H. Alfvén, "Double layers and circuits in astrophysics," *IEEE Trans. Plasma Sci.*, vol. PS-14, no. 6, Dec. 1986.
[36] O. Buneman, C. W. Barnes, J. C. Green, and D. E. Nielsen, "Principles and capabilities of 3-D, E-M particle simulations," *J. Comp. Phys.*, vol. 38, pp. 1-44, 1980.
[37] D. Nielsen, J. Green, and O. Buneman, "Dynamic evolution of a z-pinch," *Phys. Rev. Lett.*, vol. 42, pp. 1274-1277, 1979.
[38] A. L. Peratt, J. Green, and D. Nielsen, "Evolution of colliding plasmas," *Phys. Rev. Lett.*, vol. 44, pp. 1767-1770, 1980.
[39] A. L. Peratt, C. M. Snell, and H. F. Webster, "Spiral structure in magnetically confined electron sheet beams," in *Conf. Record IEEE Int. Conf. Plasma Sci.* (Pittsburgh, PA), IEEE Cat. 85CH2199-8, 1985, pp. 46-47.
[40] W. Peter, "Time-dependent interaction between space plasmas and transverse magnetic fields," *IEEE Trans. Plasma Sci.*, vol. PS-14, no. 6, Dec. 1986.
[41] W. H. Bennett, "Magnetically self-focussing streams," *Phys. Rev.*, vol. 45, pp. 890-897, 1934.
[42] H. Alfvén and N. Herlofson, "Cosmic radiation and radio stars," *Phys. Rev.*, vol. 78, p. 616, 1950.
[43] A. T. Moffet, "Strong nonthermal radio emission from galaxies," in *Galaxies and the Universe*, Sandage, Sandage, and Kristian, Eds. 1975, ch. 7, pp. 211-281.
[44] K. C. Westfold, "The polarization of synchrotron radiation," *Astrophys. J.*, vol. 130, pp. 241-258, 1959.
[45] V. L. Ginzburg and S. I. Syrovatskii, "Cosmic magnetobremsstrahlung (synchrotron radiation)," *Annual Reviews of Astronomy and Astrophysics*, L. Goldberg, A. J. Deutsch, and D. Layzer, Eds. Palo Alto, CA: Annual Reviews, 1965, pp. 297-350.
[46] V. L. Ginzburg and S. I. Syrovatskii, *The Origin of Cosmic Rays*. New York: Gordon and Breach, 1969.
[47] R. C. Bless, "The theory of synchrotron radiation," in *Nebulae and Interstellar Matter*, B. M. Middlehurst and L. H. Aller, Eds. Chicago, IL: University of Chicago Press, 1968, ch. 12.
[48] A. van Steenbergen, "Synchrotron radiation sources," *IEEE Trans. Nucl. Sci.*, vol. NS-26, pp. 3785-3790, 1979.
[49] W. K. H. Panofsky and M. Phillips, *Classical Electricity and Magnetism*. Reading, MA: Addison-Wesley, 1962, ch. 20.
[50] G. R. Burbidge, "On synchrotron radiation from Messier 87," *Astrophys. J.*, vol. 124, pp. 416-429, 1956.
[51] T. N. Lie and R. C. Elton, "X radiation from optical and inner-shell transition in a highly ionized dense plasma," *Phys. Rev. A*, vol. 3, pp. 865-871, 1971.
[52] T. J. Welch and E. J. Clothiaux, "X-ray structure of a pinched plasma in a vacuum spark," *J. Appl. Phys.*, vol. 45, pp. 3825-3827, 1974.
[53] J. Fukai and E. J. Clothiaux, "Mechanism for the hard-X-ray emission in vacuum spark discharges," *Phys. Rev. Lett.*, vol. 34, pp. 863-866, 1975.
[54] P. J. Baum, A. Bratenahl, and R. S. White, "X-ray and electron spectra from the double inverse pinch device," *Phys. Fluids*, vol. 16, pp. 226-230, 1973.
[55] B. E. Meierovich, "Electromagnetic collapse, problems of stability, emission of radiation and evolution of a dense pinch," *Phys. Reports*, vol. 104, pp. 259-347, 1984.
[56] G. Bekefi, *Radiation Processes in Plasmas*. New York: Wiley, 1966, ch. 6.
[57] B. S. Newberger, "Synchrotron radiation from self-pinched beams," Los Alamos Nat. Lab., Los Alamos, NM, Memorandum X-8(8-83)5, 1983.
[58] B. S. Newberger, M. I. Buchwald, R. R. Karl, D. C. Moir, and T. P. Starke, "Synchrotron radiation from Bennett beams," *Bull. Amer. Phys. Soc.*, vol. 29, p. 1435, 1984.
[59] G. Reber, "Cosmic static," *Proc. IRE*, vol. 30, pp. 367-378, 1940.
[60] G. Reber, "Cosmic static," *Astrophys. J.*, vol. 100, pp. 279-287, 1944.
[61] G. Reber and J. C. Greenstein, "Radio frequency investigations of

astronomical interest," *Observatory*, Feb. 1947.
[62] G. Reber, "*Cosmic static*," *Proc. IRE*, vol. 36, pp. 1215-1218, 1948.
[63] I. S. Shklovsky, "Extragalactic radio waves," in *Cosmic Radio Waves*. Cambridge, MA: Harvard Univ. Press, 1960, ch. VI.
[64] A. G. Pachoczyk, *Radio Galaxies*. New York: Pergamon, 1977.
[65] G. Miley, "The structure of extended extragalactic radio sources," *Annu. Rev. Astron. Astrophys.*, vol. 18, pp. 165-215, 1980.
[66] G. C. Perola, "Radio galaxies: Observations and theories of their extended components," *Fundamentals Cosmic Phys.*, vol. 7, pp. 59-130, 1981.
[67] W. H. Bostick, "Possible hydromagnetic simulations of cosmical phenomena in the laboratory," *Rev. Mod. Phys.*, vol. 30, pp. 1090-1094, 1958.
[68] B. Lehnert, "Plasma physics on cosmical and laboratory scale," *Nuovo Cimento*, vol. 13 (supplement), pp. 59-107, 1959.
[69] E. A. Parker, "Precise measurements of the flux densities of radio sources Cas A and Cyg A at metre wavelengths," *Mon. Notic. Roy. Astron. Soc.*, vol. 138, pp. 404-422, 1968.
[70] S. Mitton and M. Ryle, "High resolution observation of Cygnus A at 2.7GHz and 5GHz," *Mon. Notic. Roy. Astron. Soc.*, vol. 146, pp. 15-27, 1969.
[71] P. J. Hargrave and M. Ryle, "Observations of Cygnus A with the 5-km radio telescope," *Mon. Notic. Roy. Astron. Soc.*, vol. 166, pp. 305-327, 1974.
[72] A. J. Winter *et al.*, "The structure of Cygnus A at 150 MHz," *Mon. Notic. Roy. Astron. Soc.*, vol. 192, pp. 931-944, 1980.
[73] A. Toomre, "Mergers and some consequences," in *The Evolution of Galaxies and Stellar Populations*, B. M. Tinsley and R. B. Larson, Eds. New Haven, CT: Yale Univ. Observatory, 1977, pp. 401-427.
[74] G. R. Burbidge, "Possible sources of radio emission in clusters of galaxies," *Astrophys. J.*, vol. 128, pp. 1-8, 1958.
[75] V. L. Afanasiev, I. D. Karachentsev, V. P. Arkhipova, V. A. Postal, and V. G. Metlov, "Radial velocities of some interacting galaxies," *Astron. Astrophys.*, vol. 91, pp. 302-304, 1980.
[76] M. J. Cameron, "The structure of bright galaxies at 408 MHz," *Mon. Notic. Roy. Astron. Soc.*, vol. 152, pp. 439-460, 1971.
[77] A. L. Peratt and J. C. Green, "Magnetic sump formation and plasma confinement between z-pinched plasmas," in *Proc. 1981 IEEE Int. Conf. Plasma Sci.* (Sante Fe, NM), IEEE Conf. Record 81CH1640-2, 1981, p. 64.
[78] R. J. Dufour *et al.*, "Picture processing analysis of the optical structure of NGC5128 (Centaurus A)," *Astron. J.*, vol. 84, pp. 284-301, 1979.
[79] G. G. Polley and S. N. Henbest, "Observations of 48 extragalactic radio sources with the Cambridge 5-km telescope at 5 Ghz," *Mon. Notic. Roy. Astr. Soc.*, vol. 169, pp. 477-526, 1974.
[80] J. M. Riley and G. G. Polley, "Observations of 31 extragalactic sources with the Cambridge 5-km telescope at 5 Ghz," *Memo. Roy. Astron. Soc.*, vol. 80, pp. 105-137, 1975.
[81] R. T. Schilizzi and W. B. McAdam, "Observations of extended sources at 408 MHz-I. The radio structures," *Memo. Roy. Astron. Soc.*, vol. 79, pp. 1-73, 1975.
[82] A. H. Bridle, "Sidedness, field configuration, and collimation of extragalactic radio jets," *Astron. J.*, vol. 89, pp. 979-986, 1984.
[83] L. Rudnick and B. K. Edgar, "Alternating-side ejection in extragalactic radio sources," *Astrophys. J.*, vol. 279, pp. 74-85, 1984.
[84] A. G. Willis, "The large scale structure of extra-galactic radio sources (>arcsecond)," *Physica Scripta*, vol. 17, pp. 243-255, 1978.
[85] J. M. Riley and N. J. B. A. Branson, "New observations of 3C382, 3C452, and 3C465 at 2.7 and 5 GHz," *Mon. Notic. Roy. Astron. Soc.*, vol. 164, pp. 271-287, 1973.
[86] J. A. Högbom, "A study of the radio galaxies 3C111, 192, 219, 223, 315, and 452," *Astron. Astrophys. Suppl.*, vol. 36, pp. 173-192, 1978.
[87] L. Oster, "Effects of collisions on the cyclotron radiation from relativistic particles," *Phys. Rev.*, vol. 119, pp. 1444-1454, 1960.
[88] I. W. A. Browne, "MERLIN observations of superluminal radio sources," *Nature*, vol. 299, pp. 788-793, 1982.
[89] K. I. Kellerman, "Radio galaxies and quasars," *Ann. New York Acad. Sci.*, vol. 336, pp. 1-11, 1980.
[90] S. C. Unwin *et al.*, "Superluminal motion in the quasar 3C345," *Astrophys. J.*, vol. 271, pp. 536-550, 1985.
[91] R. L. Moore, J. A. Biretta, A. C. S. Readhead, and L. Baath, "Superluminal acceleration of the new component in 3C345," in *VLBI and Compact Radio Sources*, R. Fanti, K. Kellermann, and G. Setti, Eds. Dordrecht, Holland: Reidel, 1984, pp. 109-110.
[92] H. Alfvén, *Cosmic Electrodynamics*. New York: Oxford, 1950, p. 206.
[93] B. D. Turland, "Observations of M87 at 5 GHz with the 5-km telescope," *Mon. Notic. Roy. Astr. Soc.*, vol. 170, pp. 281-294, 1975.
[94] J. R. Forster, J. Dreher, M. C. H. Wright, and W. J. Welch, "Virgo A at 1.3 centimeters," *Astrophys. J.*, vol. 221, pp. L3-L6, 1978.
[95] G. D. Schmidt, B. M. Peterson, and E. A. Beaver, "Imaging polarimetry of the jets of M87 and 3C273," *Astrophys. J.*, vol. 220, pp. L31-L36, 1978.
[96] H. Andernach, J. R. Baker, A. von Kap-herr, and R. Wielebinski, "The radio continuum of M87," *Astron. Astrophys.*, vol. 74, pp. 93-99, 1979.
[97] F. N. Owen, P. E. Hardee, and R. C. Bignell, "VLA observations of the M87 jet at 6 and 2 centimeters," *Astrophys. J.*, vol. 239, pp. L11-L15, 1980.
[98] J.-L. Nieto and G. Leliévre, "High-resolution observations of M87," *Astron. Astrophys.*, vol. 109, pp. 95-100, 1982.
[99] G. Leliévre, J.-L. Nieto, D. Horville, L. Renard, and B. Servan, "Optical structures of the M87 and 3C273 jets," *Astron. Astrophys.*, vol. 138, pp. 49-56, 1984.
[100] C. Flatters and R. G. Conway, "The radio jet of the quasar 3C273," *Nature*, vol. 314, pp. 424-426, 1985.
[101] R. G. Conway and D. Stannard, "Radio brightness distribution of 3C273," *Nature*, vol. 255, pp. 310-312, 1975.
[102] R. A. Perley, A. G. Willis, and J. S. Scott, "The structure of the radio jets in 3C449," *Nature*, vol. 281, pp. 437-442, 1979.
[103] W. Baade, "Polarization in the jet of Messier 87," *Astrophys. J.*, vol. 123, pp. 550-551, 1956.
[104] G. K. Miley and H. van der Laan, "The polarization distribution of eleven 3C radio galaxies at 1415 MHz," *Astron. Astrophys.*, vol. 28, pp. 359-372, 1973.
[105] J. W. Dreher, "Polarization maps of Cygnus A at 23 gigahertz," *Astrophys. J.*, vol. 230, pp. 687-696, 1979.
[106] S. F. Burch, "Multifrequency studies of seven 3CR radio sources-II. Results and interpretations," *Mon. Notic. Roy. Astron. Soc.*, vol. 186, pp. 519-553, 1979.
[107] R. G. Strom and A. G. Willis, "Multifrequency observations of very large radio galaxies, II. 3C236," *Astron. Astrophys.*, vol. 85, pp. 36-54, 1980.
[108] A. Ferrari, "Jets in galaxies," *ESA J.*, vol. SP-207, pp. 259-273, 1984.
[109] A. H. Bridle and R. A. Perley, "Extragalactic radio jets," *Annu. Rev. Astron. Astrophys.*, vol. 22, pp. 319-358, 1984.
[110] W. Baade and R. Minkowski, "Identification of the radio sources in Cassiopeia, Cygnus A, and Puppis A," *Astrophys. J.*, vol. 119, pp. 206-231, 1954.
[111] R. I. Potash and J. F. C. Whardle, "4C 32.69: A quasar with a radio jet," *Astrophys. J.*, vol. 239, pp. 42-49, 1980.
[112] R. Linfield, "VLBI observations of jets in double radio galaxies," *Astrophys. J.*, vol. 244, pp. 436-446, 1981.
[113] B. H. Wills, "A Seyfert galaxy joins the jet set," *Nature*, vol. 313, p. 741, 1985.
[114] J. O. Burns and W. A. Christiansen, "Radio jets and bridges in luminous double sources: 3C388 and 0816 + 526," Univ. of New Mexico, Albuquerque, Rep., 1980.
[115] F. N. Owen and J. J. Puschell, "VLA observations of Jodrell Bank radio quasars," *Astron. J.*, vol. 89, pp. 932-957, 1984.
[116] R. F. Warren-Smith, D. J. King, and S. M. Scarrott, "Polarimetry and photometry of M87: Is the jet fading?," *Mon. Notic. Roy. Astron. Soc.*, vol. 210, pp. 415-424, 1984.
[117] B. E. Meierovich, "Macroscopic stability of charged particle beams," *IEEE Trans. Plasma Sci.*, vol. PS-14, no. 14, pp. 683-689, Dec. 1986.